Tectonophysics
July 2023, Volume 859, pp. 229899 (21p.)
https://doi.org/10.1016/j.tecto.2023.229899
https://archimer.ifremer.fr/doc/00836/94810/

Emplacement of a lamprophyric sheet swarm under ductile transpression in continental crust. Insights from a Variscan magmatic complex in the West Armorican belt, Western France

Le Gall Bernard [1, *], Caroff Martial [1]

[1] Géo-Ocean, Univ. Brest, CNRS, Ifremer, UMR6538, F-29280 Plouzané, France

* Corresponding author : Bernard Le Gall, email address : blegall@univ-brest.fr

Abstract :

We present structural data from a Variscan magmatic complex of dominantly lamprophyric (kersantite) and associated felsic (microgranodiorite) sheets - the West Armorican swarm (WAS) - injected into Paleozoic metasedimentary series at the western extremity of a transpressional system in the Armorican belt, Western France. The comparative structural analysis of nearly 100 individual intrusive sheets and their host-rocks demonstrates that the WAS complex is a syntectonic magmatic structure which intruded during the onset of regional shortening via successive pulses alternating with three strain episodes (D1-D2-D3). The moderate/high dipping attitude of a great majority of intrusions, along with their prominent orientation parallel to the regional cleavage (S1), i.e. orthogonal to the direction of shortening, challenge theoretical predictions about magma-filled fractures in contractional settings. These apparently atypical features are reconciled in a kinematic model which emphasizes the influence of both host-rock planar anisotropies (S1 cleavage and D3 shear patterns) and structural inheritance on magma pathways, and instead hypothesizes the negligible role of the ambient stress field. Comparisons are attempted with syncollisional lamprophyre systems present in the European Variscides, and more especially in the SE Bohemian massif.

Highlights

► Structural analysis of a lamprophyre swarm cutting through strained host-rocks. ► Magma injected during shortening in a Variscan transpressional setting, West France. ► The role of host-rock planar anisotropies on magma pathway is emphasized. ► Elaboration of a kinematic model about magma emplacement through a contracted crust.

Keywords : lamprophyre intrusive sheets, ductile strain, host-rock anisotropies, transpressional setting, West Armorican Variscides

1. Introduction

Development of collision-related orogenic belts is generally accompanied by magmatic processes which express in various ways as a function of many parameters including: (i) the magma petrology and rheology, (ii) the mode of magma emplacement (intrusive *vs* extrusive and plutons *vs* sill-dyke swarms), (iii) the depth of magma emplacement (infra- *vs* supra-crustal levels) and (iv) the strain/magmatism timing relationships (syn-, late-, post-tectonic/collisional systems). The combination of these parameters leads to a great variety of magmatic rock-types, the most of which have been widely documented worldwide. However, syncollisional (*sensu lato*) sill/dyke swarms injected during shortening through mid/upper-crustal levels have received so far very little attention. Those published in literature chiefly concern: (i) intrusions injected in lower (Cagnard et al., 2004) or shallow crustal levels (Foster et al., 2001; Galland et al., 2003; 2007a, b; Mazzerini et al., 2010; Menand et al., 2010; Montanari et al., 2010a, b; Ferré et al., 2012; Tibaldi et al., 2017), and (ii) late-post collisional intrusions emplaced during extensional/transtensional stages that commonly accompany the gravity collapse of orogenic mountains (Gapais et al., 1993; Zeitlhofer et al., 2016).

The limited number of investigated synorogenic sill/dyke networks likely reflects the generally agreed assertion that opening of vertical crack/fracture networks as potential magma feeder conduits is made difficult in contractional tectonic regimes because of the horizontal attitude of the maximum principal stress (Anderson, 1951; Glazner, 1991; Hamilton, 1995; Watanabe et al., 1999). Consequently, the mechanisms of injection and propagation of dyke intrusions in compressional environments, as well as the way the strained host-rocks

accommodate their emplacement, are not yet fully understood (e.g., Schoffield et al., 2012; Bertelsen et al., 2018; Kjoll et al., 2019).

The aim of our work is to partly fill this gap by presenting structural results about a magmatic swarm emplaced during the Variscan orogeny in a transpressional setting at the western extremity of the Armorican belt, Western France (Fig. 1d). The so-called West Armorican swarm (WAS) is a lamprophyric complex composed of kersantite and microgranodiorite sheet-like intrusions (Caroff et al., 2021) cutting through deformed Paleozoic metasedimentary series in the Brest syncline (Figs. 1d, 2). The main goals of our field-based study are: (i) to characterize the main geometric attributes (strike, dip, width, spacing, ..) of ca. 100 individual intrusions continuously exposed along coastal sections in the Brest bay (Fig. 2), (ii) to precise their spatial and temporal relationships with the polystrained metasedimentary host-rocks, and (iii) to qualitatively discuss still challenging issues about the competing role played by various physical parameters on the trajectory and final shape of individual intrusions. Lastly, the structural significance of the WAS complex is discussed with regards to the lamprophyre and/or syncollisional intrusive sheet networks present: (i) in the Armorican belt and (ii) in the entire European Variscides, with emphasis on the Bohemian systems which display a wide range of temporal patterns and structural settings.

1. Geodynamical and geological settings

The Variscan belt in Europe is composed of a mosaic of continental blocks which collided separately, after multiple and diachronous oceanic subductions (e.g. von Raumer et al., 2014). That resulted in an intricate pattern of orogenic segments displaying their own tectonic and magmatic histories (e.g. Kroner and Romer, 2013). During Carboniferous times, the oblique convergence of the Gondwana and Laurussia plates induced a large-scale transpressional setting in the intervening Armorica micro-plate, at the western extremity of the orogeny

(Gumiaux et al., 2004; Ballèvre et al., 2009). Transpression chiefly expressed by dextral ductile wrenching along the North and South Armorican shear zones (NASZ, SASZ) and their satellite structures (Elorn, Monts d'Arrée and Montagnes Noires shear zones, ESZ, MASZ and MNSZ, respectively, in Fig. 1d), in response to a NW-SE-directed shortening (Gapais and Le Corre, 1980; Darboux and Le Gall, 1988; Le Gall et al., 1992; Gumiaux et al., 2004; van Noorden et al., 2007). These crustal-scale discontinuities currently separate high-grade metamorphic and plutonic terrains in the North and South Armorican domains (in addition to Cadomian basement rocks in the North) from a thick pile (>5 km) of Late Proterozoic-Paleozoic low-grade metasedimentary rocks, pierced by granitic intrusions, in a central domain (CAD, Fig. 1d). At the western extremity of the CAD (WCAD), the moderate amount of strain resulted in a map-scale syncline pattern (Brest and Châteaulin) which was the locus of the WAS magmatic complex under study (Figs. 1d, 2). The age of the onset of strain in the WCAD is approximated to ca. 315 Ma by correlations with the age yielded by synkinematic granites (Saint-Renan, Huelgoat) along the NASZ and MASZ, respectively (Fig. 1d) (Le Gall et al., 2014; Ballouard, 2016). These tectono-magmatic events are nearly synchronous to the peak of metamorphism in the adjoining LMD (Figs. 1d, 2) (Schulz, 2013; Marcoux et al., 2009; Authemayou et al., 2019).

The Brest syncline extends as a 25 x 50 km^2 bowl-like fold, south of the Elorn bounding shear zone (Fig. 2). Its progressive narrowing westwards (from 50 to 30 km) is accompanied by the counterclockwise rotation of the regional structural grain from N90°E to N60°E. The ca. 3 km-thick succession of Paleozoic metasedimentary series involved in the Brest syncline ranges in age from Ediacaran/Cambrian (Brioverian) up to Late Devonian (Fig. 2b) (Chauris et al., 1980; Babin et al., 1982). Their lithological content can be simplified into two contrasted categories.

A ca. 1200 m-thick lower lithostratigraphic part (Ordovician-Lower Devonian) is dominated by competent series, including the Armorican Sandstone Fm. (<200 m), the Plougastel Schist and Quartzite Fm. (400 m), the Landevennec Sandstone Fm. (100 m) and the Armorique Limestone Fm. (100 m). They are extensively exposed to the north in a 5 km-wide belt of regional-scale folds whereas only part of them form a monoclinal structure along the southern limb of the syncline (Figs. 2a, c). The axial part of the syncline is occupied by a ca. 1000 m-thick succession of dominantly fossiliferous schist series, Middle-Late Devonian in age, which are the preferential locus of WAS intrusions (Fig. 2a, Chauris et al., 1980; Babin et al., 1982; Castaing et al., 1987; Plusquellec et al., 1999; Darboux et al., 2010). A thorough petrographic analysis of the kersantite and microgranodiorite populations, as well as their geochemical affinities and the nature of the source material, have been recently performed by Caroff et al. (2021). The texture and mineral assemblages of these rocks show limited variations. Kersantites are a fine-grained to moderately coarse-grained material predominantly made up of plagioclase and dark micas, and subsidiary carbonates and secondary quartz. The microgranodiorite material is an aphanitic or quartz-phyric fine-grained leucocratic rock made up of oligoclase, generally albitized or damouritized, quartz, K-feldspar, chloritized biotite and muscovite. Kersantite/microgranodiorite cross-cutting relationships are exhibited at three sites (Rosmellec, Ile Longue, Porsguen; Fig. 2a, Supplementary Material Fig. S1). Though the kersantite material systematically intrudes (and post-dates) microgranodiorite, the cogenetic origin of the two types of magma is argued from petro-geochemical evidence discussed in Caroff et al. (2021).

The WAS complex has not yet benefitted from radiometric dating because of unfavorable mineralogy. However, a maximum age is provided by the few kersantite sheets cutting through Visean/early Serpukhovian series in the Châteaulin syncline to the SE (Fig. 2a, Doubinger and Pelhate, 1976). These relative timing data invalidate previous interpretations

of the WAS intrusions as syncompressional magmatic structures related to an early (Late Devonian) orogenic event (Rolet and Thonon, 1978). These structural and temporal issues are fully discussed in the present work.

Addressing the development of the WAS magmatism in the West Armorican Variscan context first requires to discuss the still debatable nature of the structural relationships between the LMD and the WCAD. This issue is illustrated by the sketch structural cross-section in Fig. 1e, elaborated by combining available metamorphic data (Jones, 1994; Schulz, 2013) with recent structural onshore/offshore results (Le Gall et al., 2014; Authemayou et al., 2019).

North of the pyrophyllite-bearing facies in the Brioverian series, the LMD metamorphic terrains are involved in a southerly-inclined monoclinal pattern on the southern flank of the LMD dome. Their mineralogical assemblages typically reflect epizonal-mesozonal P/T conditions that increase gradually northwards from chlorite-bearing facies to biotite, staurolite and sillimanite/migmatite facies in the structurally lower part of the pile. No gap, neither reverse position of metamorphic rock-types is observed in the pile (Jones, 1994; Schulz, 2013). To the south, the Brioverian series pass, without any stratigraphic gap (despite the presence of the ESZ), into Paleozoic pyrophyllite-bearing series in the Brest syncline (Paradis et al., 1983).

A quite similar tectono-metamorphic arrangement occurs on the eastern edge of the Leon dome (Fig. 1d, Le Gall et al., 2021). The only regional-scale structures so far identified at the LMD-WCAD transition zone are discrete dextral shear zones cutting through either the Brest orthogneiss (Pierres Noires shear zone, PSZ) or Ordovician quartzites of the Armorican sandstone Fm. along the northern flank of the Brest syncline (ESZ; Fig. 1e). In contradiction with previous allochthonous-type models (Balé and Brun, 1986; Rolet et al., 1986; Faure et al., 2008, 2010; Ballèvre et al., 2009), the southern part of the LMD and the adjoining WCAD are here regarded as sub-autochthonous infra- and supra-crustal domains, respectively,

forming a quasi-continuous and coherent crustal section on the southern limb of the Leon dome. Their boundary is thus necessarily arbitrary and located here in the Brioverian series (Fig. 1e).

By further assuming that the lack of Lower Paleozoic sedimentary series in the LMD is not due to erosion (excepted in the South Ouessant island, see Caroff et al., 2016, 2020, for details), it is also inferred that in pre-Variscan times the proto-LMD formed an elevated domain in the uplifted footwall block of the proto-Elorn extensional fault bounding to the north the long-lived (> 100 Ma) and subsiding WCAD basin.

2. Methodology

Our work is built on a field-based structural study devoted to both WAS intrusions and their strained metasedimentary host-rocks in the Brest syncline. Because of very poor inland exposures, field investigations have been restricted to the indented coastal section continuously exposed on the NE edge of the Brest bay (Fig. 2c). Our structural data are synthetized on a ca. 20 km-long cross-section perpendicular to the regional structural grain. The spatial and temporal relationships of strain and intrusion development are described in details by a careful field structural analysis. Each type of ductile deformation is defined in terms of geometry, relative chronology and spatial distribution along the reference section. In parallel, the orientation, dip attitude and width of ca. 100 individual magmatic (kersantite and microgranodiorite) intrusions have been measured. Each intrusive sheet is assigned the letter *K* (kersantite) or *μGD* (microgranodiorite) and a unique number (1-101 from W to E on the coastal cross-section in the Supplementary Material Fig. S1). Many of them are shown on the figures with their corresponding number. All the sites mentioned in the text are located on the Google Earth map in the Supplementary Material Fig. S1. Our 2D-cross-sectional work does not permit to investigate the length dimensions and map-scale geometry of the intrusions, excepted about the Ile Longue laccolith at the western edge of the syncline, and on a few

rocky platforms intermittently exposed at high magnitude low tides (Château, Le Roz, Yelen, Fig. 2a). From cross-cutting relationships with the poly-strained host-rocks, different generations of intrusions are discriminated as pre-, syn-, and post-strain bodies with regards to three successive strain events detailed below. Both the kersantite (88%) and microgranodiorite (12%) material are considered as two homogeneous petro-geochemical populations (Caroff et al., 2021). However, at a few localities (North Château), geochemically distinct kersantite intrusions are distinguished because, as being further involved in structures with contrasted styles, they supply supportive evidence for successive pulses of magma at various stages of ductile strain.

Some clarifications are needed about the terms "sills and dykes" commonly used about sheet intrusions. In most of published papers, the host-rocks consist of unstrained and flat-lying (layered) sediments or volcanics formed in extensional settings. Therefore, because of their conventional definition as intrusions either concordant with or secant to host-rock anisotropies, sills and dykes are routinely considered as horizontal or inclined/vertical magmatic features, respectively. These notions are inadequate about the WAS intrusions under study because, as intruding through folded strata, a given intrusion may lie as a sill-like body in one place and then extends laterally as a dyke-like body. These notions are substituted by the terms "shallowly-inclined (SIS), moderately-inclined (MIS) and highly-inclined (HIS) sheets", for dipping attitudes (∂) arbitrarily set at $\partial \leq 30°$, $30° < \partial \leq 60°$ and $\partial > 60°$, respectively. This nomenclature is justified by the fact that most of WAS intrusions, though being interpreted as syn-collisional magmatic structures, chiefly escaped deformation and thus intruded with their present attitudes.

3. Results

The nature of parameters that might have influenced the emplacement, propagation and final architecture of the WAS magmatic intrusions is addressed below in relation with: (i) the kersantite *vs* microgranodiorite composition of the magma and (ii) the mechanical behavior of the competent (grits, quartzites, limestones) *vs* weak (schists) host-rocks during deformation in the Northern *vs* Southern units. Others potential controlling factors such as tectonic stress and magma properties are not addressed in the present work.

4.1. The host-rock ductile strain pattern

The 2D-structure of the Brest syncline on the cross section in Fig. 2c is derived from published geological maps further combined to our own structural field data. It corresponds to a highly asymmetrical and two-fold structure comprising of: (i) a Northern unit, chiefly composed of competent and folded Ordovician-Lower Devonian series, juxtaposed to the south along the SE-directed Rozegat thrust to (ii) highly-sheared Middle-Upper Devonian schist series (Southern unit) that in turn pass southwards into the unfaulted and monoclinal flank of the syncline.

The overall structure of the Northern unit is dominated by a succession of km-wavelenght upright or overturned syncline/anticline folds (D_1 event) (Fig. 2c). Anticline hinge zones are commonly cored by massive quartzitic strata of the Plougastel and Landevennec Fms. Axes of D_1 parasitic folds exposed in the field plunge shallowly (<10° in average), mostly in the SW quadrant (Fig. 3a). D_1 folds are associated with a steep penetrative axial-plane cleavage (S_1), oriented in the range 20-60° (Figs. 3a, b). It is noteworthy that the S_1 planes do not bear any apparent stretching lineations. The Middle/Upper Devonian schist series that locally extend in the associate synclines show a more intricate geometry resulting from overprinting of S_1 planes by D_2 folds, in turn disrupted by a shallowly-inclined network of shear surfaces (D_3 event). A decoupling level, not yet argued in the field, is suspected to occur between the lower

(competent) and upper (schist) series (Fig. 2c). Both the D_1 and D_2 fold patterns are disrupted by a system of shear and ramp-thrust structures displaying prominent transport directions to the east and assigned to a D_3 event. A few of these dominantly shallowly-inclined structures are sites of magma injection (Sections 4.2.5, 4.3). From the cut-off geometry of footwall/hangingwall stratigraphic limits, thrust displacements are assumed not to exceed 100 m's, excepted about the Rozegat frontal thrust where they are <500 m (Fig. 2c). The northernmost thrust structures might merge at depth along the Elorn bounding dextral shear zone in a regional-scale flower pattern.

The Middle-Upper Devonian series in the Southern unit show a more intricate structural pattern resulting from the superimposed effects of three ductile strain events (Babin et al., 1975). A shallowly/moderately-dipping prominent cleavage (S_1) represents the axial plane of overturned to recumbent folds (Fig. 3c), correlated to D_1 structures. Again, the S_1 surfaces do not bear any stretching lineation. The wide distribution of S_1 strikes, with a peak in the range N50-100°E (Figs. 3d1, e), is due to a second generation of dominantly upright and shallowly-plunging (<30° in average) folds, assigned to a D_2 event. The density of S_1 poles in Fig. 3d2 indicates a mean D_2 fold axis plunging at ca. 30° to N240°E, in agreement with field observations. The D_1-D_2 multistage fold pattern is disrupted by a network of SE-directed flat-lying shear structures (event D_3), frequently accompanied by tectonic schist breccias. Their thrust origin is locally argued, as for example at the Kerloziou site where Upper Devonian schists are tectonically overlain by Middle Devonian series along a nearly horizontal contact (Fig. 3f; Babin et al., 1975). Lastly, these early ductile planar fabrics are involved into a succession of a few km's-wavelength undulations, possibly formed on top of a blind ramp-thrust system involving the Lower Paleozoic competent series at depth (Fig. 2a).

The lack of pre-Devonian series currently exposed in the Southern unit may be likely related to the decoupling level envisaged in the Northern unit (Fig. 2a). Dextral strike-slip tectonics is

restricted to the axial part of the Brest syncline, in relation with the so-called Le Roz shear zone (Figs. 2a, c). This structural feature further coincides with a major magmatic structure discussed in Section 4.2.6.

4.2. The WAS intrusive complex

4.2.1. Spatial distribution

Because of limited exposures inland, very little is known about the spatial distribution and map-geometry of WAS intrusions. They are thus drawn as discrete point-like features on published 1: 50 000 geological maps (Fig. 2a; Chauris et al., 1980; Babin et al., 1982; Castaing et al., 1987; Plusquellec et al., 1999; Darboux et al., 2010). New insights are here provided about their amount, location, spacing and density from the 20 km-long coastal reference cross-section (Figs. 2a, 4a), thought to be representative of the WAS complex as a whole.

Along the analyzed section, kersantite are more widespread than microgranodiorite intrusions. The latter are mostly restricted to two main areas (Caro and Le Roz/Ile Longue) which further coincide with the greatest concentration of intrusions in each structural unit. The main cluster of intrusions (x20) occurs in the Le Roz area, i.e. in the axial part of the Brest syncline, from which the intrusion frequency decreases gradually in a symmetric way. In contrast, in the Northern unit, the frequency of intrusions decreases asymmetrically southwards from a maximum peak (x10) in the Caro area. The spatial association of the Le Roz/Ile Longue highly intruded zone with a major dextral shear zone is discussed in Section 4.2.6.

4.2.2. Strike and dip

The orientation (dip and strike) of planar intrusions is a key-parameter for identifying realistic geometries with respect to the ambient tectonic stress/strain fields. The strike pattern

of nearly 100 individual magmatic sheet intrusions measured in the field is plotted on the rose diagrams in Figs. 4b-d. Intrusion strikes display a dominant regional trend in the range N20-100°E (ca. 65%), with three peaks at N40-50°E, N70-80°E and N90-100°E (Fig. 4b). They rotate clockwise from N30-50°E in the Northern unit (Fig. 4c) to N80-100°E in the Southern unit (Fig. 4d). This intrusion strike changing is fairly consistent with variations of S_1 cleavage orientations in the Northern and Southern units. Subordinate intrusion networks (15%) strike N120°E (in both units) and N160°E (Southern unit) (Figs. 4b-d).

On the diagram in Fig. 4e, the dip pattern (∂) of 95 intrusions is scattered between 10° and 90°, with two peaks in the intervals 30-50° (33%) and 80-90° (19%) for both kersantite and microgranodiorite material, and irrespective of the host-rock lithology (competent *vs* schist). With regards to the nomenclature adopted above, the HIS ($\partial > 60°$) and MIS ($30° < \partial \leq 60°$) populations (40% and 50%, respectively) largely exceed those of SIS ($\partial < 30°$, 10%).

4.2.3. Width

Most of WAS intrusions are tabular bodies showing sharp contacts with the deformed metasedimentary host-rocks. Width measurements (x101), made normal to their walls, have been analyzed by frequency distribution as a function of: (i) their kersantite *vs* microgranodiorite nature and (ii) their dipping attitude. The measured widths are mostly in the range 0.2-30 m with 65% <5 m (Fig. 4f). The proportion of microgranodiorite *vs* kersantite is higher for widths >25 m. In contrast, no direct correlations exist between the width values and: (i) the dipping attitude of the intrusions and (ii) the host-rock lithologies. Except for the Le Roz/Ile Longue highly-intruded zones (Section 4.2.6), it appears that the areas of greatest widths (Goasquellou, Rosmellec, Squiffiec; Fig. 2a) do not strictly coincide with areas of high frequency. Neither significant (decreasing) width changes have been observed at increasing distances from the contact of these two zones.

4.2.4. Ring-shaped intrusions

Three kersantite intrusive sheets, cutting through Upper Devonian schists (Porsguen Fm.) on the southern edge of the Château beach, form map-scale elliptical structures (40 x 60 m), aligned over a distance of 300 m along a N140°E axis parallel to their marked elongation (Fig. 5a). The two southern ones ($K_{55, 56}$) form ring-shaped structures which evoke those more routinely observed in younger volcanic belts (Takada, 1988; Walker, 1999; Pasquare and Tibaldi, 2007). Each ring-shaped structure is formed by a 6 to 8 m-wide peripheral intrusion, dipping moderately inward on its NE flank and passing into a vertical position on its SW flank. These ring-shaped intrusions are unstrained and show a still preserved and regularly-spaced cooling joint pattern orthogonal to their margins. The third intrusion (K_{54}) forms an elongated plug oriented at NE-SW. All the intrusions are wrapped by the regional S_1 cleavage.

4.2.5. Transition patterns from highly- to shallowly-inclined sheets

Spatial variations of intrusion trajectories from HIS to SIS are observed in two localities. In the South Château area, a kersantite dyke (K_{59}), >10 m-wide, passes laterally westwards and upwards into a subhorizontal intrusive sheet, in turn underlain by a top-to-N155° shear surface (D_3) and associated asymmetrical fold structures in the underlying Famennian schist host-rocks (Fig. 5b). Along the Caro section (Fig. 5c), a top-to the west and shallowly-dipping shear surface (D_3) is cut at high angle by a 4 m-wide microgranodiorite HIS (μGD_{17}) which displays a 20 cm-thick apophysis along the trace of the shear surface over a distance of 20 m.

4.2.6. The Le Roz and Ile Longue magmatic zones

The morphology of the Le Roz peninsula provides a 3D-view of magmatic and tectonic structures along two orthogonal cliff sections and over the 250 x 100 m^2 adjoining rocky platform (Fig. 6a). On the EW-trending section (Fig. 6b), two distinct tectono-magmatic packages are tectonically juxtaposed. The upper one is composed of a subhorizontal and nearly undeformed microgranodiorite SIS (μGD_{60}), >20 m in width (its upper margin is not observed). Its lowermost part is disrupted by a series of top-to-the-W shear planes, probably related to a basal thrust contact (D_3) with an underlying assemblage of highly-strained Late Devonian schists (Porsguen Fm.) containing closely-spaced kersantite intrusive sheets. >30 % of the rock mass on the 200 m-long section in Fig. 6c is made of 3 to 10 m-wide kersantite sheets (x18, $K_{62\text{-}79}$). It further coincides (in its central part) with a high strain shear zone spectacularly expressed in both the schist host-rocks and the intrusive network. The Porsguen schists occur as tectonic breccias due to intense shearing of the folded (D_2) S_1 cleavage. The kersantite sheets form a series of disrupted and relatively steep magmatic bodies, with variable dimensions and shapes, wrapped by the brecciated schist host-rocks (Figs. 6a, c). It is noteworthy that the greatest dismembered sheet intrusions are devoid of any internal deformation and still display regular 3D-shapes bounded by the initial magmatic margins (long dimensions) and cooling joint patterns at their extremities (Figs. 6c, d). Smaller kersantite bodies form either blocks, ranging in diameter from a few dm's to a few m's in schist breccias (Fig. 6e), or elliptical boudin-like lenses surrounded by the schist breccia. The great concentration of intrusions along the Le Roz section, along with their dominant steeply-dipping attitude (inferred to be a primary feature), are considered as supportive evidence for a potential magmatic feeder zone (Le Roz) in the axial part of the Brest syncline.

A nearly similar intricate tectono-magmatic pattern is exposed in the Ile Longue area to the SW (Fig. 7). There, two contrasted tectono-magmatic packages, involving only microgranodiorite material, are tectonically juxtaposed. The upper package comprises a >30

m-wide microgranodiorite SIS resting horizontally along a basal sheared contact over flat-lying Upper Devonian schists (Porsguen Fm.) (Figs. 7a, b) (Thonon and Rolet, 1982). This laccolith-like sheet, which represents the only map-scale intrusion in the WAS complex, is cut by a few kersantite HIS. This upper package is thrusted over similar schist series which conversely display a steeply-dipping S_1 cleavage locally involved in a 100 m-wide and N70°-oriented strike-slip shear zone (Fig. 7c). The dextral sense of shearing is deduced from the asymmetry of D_2 folds superimposed on the S_1 cleavage. The shear zone encloses numerous discrete bodies of microgranodiorite material showing various dimensions and shapes, but generally forming elongated lenses surrounded by the S_1 cleavage (Fig. 7b). From their structural similarities, the Ile Longue and Le Roz tectono-magmatic patterns are laterally correlated, being dextrally-offset (>10 km) along a transverse fault (FT) still expressed in the bathymetry of the Brest bay seafloor (Fig. 2a).

4.3. Strain/intrusions spatio-temporal relationships

Timing and conditions of emplacement of the WAS magmatic intrusions are constrained by intersection relationships with host-rock planar anisotropies. Emphasis is put below on the strata pattern (S_0), principally about the competent series in the Northern unit, and on the S_1 cleavage (D_1) and flat-lying shear plane (D_3) patterns in both units (Fig. 8a; Supplementary Material Table S1). The moderate amount of intrusive sheets (10 out of 26) occurring parallel with strata in the competent series of the Northern unit indicates that strata boundaries (S_0) play a modest role on sheet trajectory. A quite different structural configuration is observed in the dominantly schist series where about 50% of intrusions (44 out of 100) are seen to follow the trace of the S_1 fabrics, whatever their shallowly- (x4), moderately- (x21) or highly- (x19) dipping attitude. Lastly, a total of 13 intrusive sheets occur along flat-lying shear zones (D_3). Three of them have been described above about the South Château and Caro HIS/SIS

transition patterns (Figs. 5b, c), as well as in the Le Roz/Ile Longue shear zone (Figs. 6, 7). One additional example is described below along the Larmor section.

The relative chronology of magma emplacement *vs* deformation events has been established about 82 (out of 101) individual intrusions which either pre-date or post-date one of the three strain episodes (D_1, D_2, D_3, Fig. 8b). The chronology of the remaining intrusions (x19) is not constrained. It is noteworthy that intrusive sheets post-dating the late shearing event (D_3) have not been documented in the WAS complex.

Only 35 intrusions display a maximum and a minimum time limits and are thus fully calibrated. Two distinct strain/intrusion temporal patterns are distinguished. (i) Intrusions emplaced at an early stage of the polyphase strain history (x20) are reported in two distinct, but closely spaced sites.

At the South Château site, the trajectory of the steeply-dipping S_1 cleavage of the host-rocks is moulded around kersantite sheets (x5), whatever their shape as either one elliptical plug (K_{54}), ring-sheets ($K_{55\text{-}56}$) or submeridian sheets ($K_{57\text{-}58}$) (Fig. 5a). The boudinaged structure of the latter, as well as triple junction trajectories of the S_1 cleavage at the extremities of individual sheets, resemble patterns studied elsewhere (Pons et al., 1995) and typically characterize synchronous magmatic and ductile strain (D_1) events. Further south in the Le Roz area, highly-strained (boudinaged) kersantite sheets (x18, $K_{62\text{-}79}$, Fig. 6) are similarly wrapped by the S_1 cleavage which, here, further recorded intense dextral shearing (D_2). These structural features again show that magma injection operated at a relatively early stage of strain, in the time-span D_1/D_2, prior to the thrust emplacement (D_3) of a nearly unstrained microgranodiorite sheet (μGD_{60}, see above Fig. 6). It is thus demonstrated that multistage injections of compositionally distinct magmas occurred at successive stages of the polyphase ductile strain history in the Le Roz area. A similar timing pattern, but involving only kersantite material, is documented at the Château site. The map and cross-section in Fig. 9

show a 30 m-wide HIS (K_{51}), parallel to the vertical S_1 cleavage in Late Devonian schists (Traonliors Fm.) and enclosing schist enclaves (inferred to correspond to S_1), which is thus interpreted as a post-D_1 intrusion. Further west, flat-lying schists occurring in the thrusted (D_3) western limb of a D_2 fold are intruded by a geochemically distinct SIS kersantite (K_{53}) (Caroff et al., 2021), again parallel with the S_1 cleavage, but here in a flat-lying attitude. The post-D_1 emplacement of the two distinct kersantite sheets likely took place prior (K_{51}) and later/during (K_{53}) the folding (D_2) and shearing (D_3) episodes, at a time when the two corresponding magmas were not connected.

Additional supportive evidence for magma injection in the time range (D_1-D_3) are provided by much less intricate structural patterns involving only one individual intrusive sheet. At the Squiffiec site (Fig. 10b), a microgranodiorite HIS (μGD_{53}) enclosing schist (S_1) enclaves post-dated the D_1 event and is in turn involved into, and thus post-dated by, a D_3 shear thrust structure. A similar sequential timing pattern is observed at the Kerascoet site where a >20 m-wide kersantite SIS (K_{87}) containing a S_1 schist enclave is disrupted along its basal contact by a flat-lying shear thrust (D_3) directed to the north (Figs. 11a, b).

(ii) The latest intrusion network (x7) identified in the WAS complex is genetically related to D_3 shear structures. Two examples have been described above about the South Château and Caro HIS/SIS transition patterns (Figs. 5b, c). In the latter site, folding of the microgranodiorite layering in the SIS apophysis ($\mu GD17$ in Fig. 11c) attests that the felsic magma was not yet frozen during the last increment of shearing. But, the most demonstrative example of syn-D_3 intrusion is exposed at the Larmor site. It corresponds to a 3 m-wide kersantite SIS (K_{23} in Fig. 10c) intruded along a shallowly-inclined and SE-directed thrust fault (D_3) cutting through vertical folded (D_1) quartzite strata (Landevennec Fm.). The kersantite SIS is locally disrupted by satellite D_3 shear zones probably formed at a late stage of the shearing event (Fig. 10d).

The partly-bracketed intrusion population (x44) also supplies fruitful insights as demonstrating that >50% of sheets (x26) post-dated the main ductile events D_1/D_2 and thus intruded at a relatively late stage of the polyphase strain history. This assertion is based on: (i) the presence of schist xenoliths (inferred to contain the S_1 dominant cleavage) within the magmatic bodies, (ii) the slight angular obliquity of the intrusion and the host-rock cleavage (S_1 or S_2), and (iii) the disruption of syncleavage fold structures (D_1 or D_2) by intrusions. The example exposed at the Yelen site (Fig. 10a) shows a 2 m-thick kersantite sheet (K_{83}) cutting at high angle through a D_2 upright fold hinge and then following the S_1 cleavage on the limb of the fold. A different fold/sheet intersection pattern is observed at the Kerdreolet site (Fig. 2a) where the trajectory of a kersantite sheet through folded schist/limestone alternations (Bolast Fm. in Fig. 2b) is offset into two linear segments in the hinge zone of a D_2 upright fold. The upper time-limit of these post-D_1/D_2 intrusions, and more specifically their temporal relationships with the D_3 strain event, is not constrained (Fig. 8b). In a symmetric way, 21 pre-D_3 intrusive sheets do not display lower time-limits, so that their emplacement prior to the early D_1 strain event cannot be excluded.

4.4. Strained *vs* unstrained intrusive sheets

Most of WAS intrusions are tabular sheets showing sharp contacts with the strained host-rocks. One of their fundamental structural features is that they escaped pervasive ductile strain (with the exception of the folded μGD_{17} SIS intruded along a D_3 shear plane). On one other hand, the involvement (or not) of intrusive sheets in brittle strain is a discriminant parameter for identifying two distinct populations. A few strained intrusive sheets have been described above in relation with low-angle shear thrust structures (D_3), but, the great majority of them are restricted to the Le Roz-Ile Longue dextral shear zone (in addition to a few sheets in the South Château area). As shown above in Fig. 6, the spectacularly dismembered (boudin-like)

geometry of the kersantite sheet network in the Le Roz shear zone (K_{63-77}) resulted from the combined effect of shear-related stretching, acting in two orthogonal directions. The horizontal stretching is assigned to dextral strike-slip shearing kinematically consistent with the asymmetry of D_2 isoclinal folds. The lack of any penetrative strain in the magmatic bodies, their disruption along cooling joints, and their preserved tabular shape (Fig. 6) indicate that the kersantite sheets have been disrupted during high strain brittle shearing during the D_2 event.

Outside the Le Roz shear zone, the sharp and wedge-shaped geometry of a number of intrusion tips, such as the MIS *K56* in the South Château ring-sheet network (Figs. 5a,12b), shows that they also behaved in a brittle way during shortening. Similarly, the brittle mechanical behavior of the strained metasedimentary host-rock during magma injection is locally documented by crack/fracture networks thought to have opened by shear failure ahead of intrusion tips (*K24* in Fig. 12a). Convincing evidence for the brittle behavior of the host-rocks during shortening have been reported above about the late low-angle shear plane pattern (D_3). Additional support is provided by a widely distributed system of narrow (30-40 cm-wide) shear zones following the walls of many intrusions (Fig. 12c). Their magmatic *vs* tectonic origin can be questioned since magma injection is also known to induce compressional strain in host-rocks (Tibaldi et al., 2017). In the present case, the unique sense of shearing (deduced from the sigmoid geometry of the S_1cleavage) on both sides of the intrusions confirms its tectonic origin. A demonstrative example is shown in Fig. 12c about a kersantite SIS (*K5*) at the Ilien ar Gwen site. Senses of shearing are not consistent regionally and might result from local stress disturbances along individual intrusive bodies. This discrete shear zone pattern was likely promoted by high rheological contrasts in the rock volume between the resistant intrusive sheets and the weaker schist host-rocks.

5. Discussion.

The structural results obtained about the WAS intrusions are discussed in two complementary ways. The first step is to evaluate whether they provide valuable constraints to better understanding the way intrusive sheet networks can intrude and propagate through a mid/upper crust recording shortening. The second step is to address the structural significance of the WAS complex in the Variscan orogeny by comparing its mode of injection with: (i) contemporaneous and/or compositionally similar magmatic intrusions present in the Armorican belt, and (ii) lamprophyre-type intrusive sheet swarms widespread elsewhere in the European Variscides, and more especially in the Bohemian massif.

5.1. Emplacement of intrusive sheets in a transpressional setting

The type of strain regime is known to be one of the governing parameters that control the trajectory and final geometry of sheet intrusions in crustal levels recording shortening (Lister and Kerr, 1991; Watanabe et al., 2002; Sibson, 2003). The transpressional setting displayed by the WCAD during the Variscan orogeny has been briefly evoked above (Section 1). It can be better defined in terms of strain regime when comparing the resulting structural patterns in both the Brest syncline and the adjoining LMD to the north. The two domains show highly contrasting tectonic styles. In the LMD, the main ductile event, i.e. the regional foliation (correlated with S_1 in the WCAD) which formed prior to exhumation path and doming processes, is characterized by planar/linear and linear (S/L- and L-types) fabrics (Authemayou et al., 2021). The corresponding NE-SW stretching lineation is associated to both wrench dextral shearing and top-to-the-NE tangential (thrust) shearing. This strain pattern has been approximated to an oblique/to/lateral flow produced by the interplay of strike-perpendicular shortening and orogen-parallel stretching. By contrast, the deformed Paleozoic series in the WCAD consistently show planar ductile fabrics (S-type, S_1/S_2 cleavages), devoid of any

linear fabrics (Section 4.1), which are typically indicative, at first approximation (without any accurate strain markers), of a plane strain regime under a strike-normal shortening.

The juxtaposition of these two structurally distinct domains suggests a strain partitioning process, further associated to a major decoupling mechanism, possibly *via* the ESZ (Fig. 13a). The strain model applied to the WCAD has major implications on the conditions of magma injection in the WAS complex. It implies that the opening of the orogen-parallel (N50-100°) magma-filled fracture network (ca. 50 %) did not occur in response to any (D_1) regional stretching. This assertion agrees with the strain/intrusion temporal pattern applied above which shows that >70% of intrusive sheets are post-D_1 magmatic features. In these conditions, two alternative driving mechanisms might be responsible for the orientation and opening of the orogen-parallel magma-filled fracture network in the WAS complex. Firstly, it has been demonstrated above that: (i) 40% of WAS intrusions are oriented parallel to the regional S_1 cleavage and (ii) they were emplaced as either syn- S_1 (Le Roz shear zone) or post-S_1 structures. It has also been shown that 13 shallowly-dipping intrusions follow the trace of D_3 shear zones. It thus clearly appears that host-rocks tectonic anisotropies played a crucial role on the propagation of magma whatever their (pre- or syn) origins with regards to the successive magmatic pulses. Interplays of shearing and magma injection are conceivable because of the lubricant behavior usually attributed to shear planes (Hollister and Crawford, 1986). Though no data yet exist about magma properties and ambient tectonic stresses, it can be reasonably hypothesized that magma overpressure acted as a potential driving force during magma injection, provided that: (i) it overcame the applied tectonic stresses, (ii) it was equal to or higher than the vertical stress (Goulty, 2005), and (iii) it was sufficient to counter the normal stress on planar discontinuities (Delaney et al., 1986; Meriaux and Lister, 2002). This hypothesis agrees with similar studies showing that magma pressure can promote upward migration of magma through upper crustal terrains subject to shortening (Tibaldi, 2005).

Two alternative driving mechanisms of magma injection are envisaged when considering the earliest magma-filled fracture network coeval to the S_1 event, i.e. those present in the South Chateau and Le Roz sites. At the South Chateau site, the N120-140°E-oriented intrusions, at high angle to the regional sheet swarm, likely originated as vertical tension-gashes, parallel to the shortening direction (Fig. 13a). These are the only WAS magmatic structures compatible with the regional shortening pattern and thus consistent with theoretical models (Anderson, 1951; Glazner, 1991; Hamilton, 1995; Watanabe et al., 1999). By contrast, the orogen-parallel strike of syn-S_1 intrusions in the Le Roz feeder/shear zone (Fig. 6) does not fit with theoretical predictions. From regional considerations, structural inheritance is regarded as a second possible driving mechanism for magma emplacement in one specific part of the WAS complex. On the sketch structural maps in Figs. 13a, b, the similar orientations and (dextral) kinematics of the ESZ, Le Roz and MASZ structures suggest that they belong a common regional fault pattern. Therefore, the inherited (Early Paleozoic) origin of the ESZ (Section 1) should also apply to the Le Roz and MASZ structures. These colinear structures likely nucleated along a N70°E-oriented discontinuity and later acted as magmatic feeder zones for lamprophyric and granitic syntectonic magmas, respectively, while recording high strain dextral shearing (Fig. 13). The fact that high-strain shearing spatially coincided with the Le Roz magmatic feeder zone is thought not to be fortuitous and might be assigned to focusing of strain in a crustal portion thermally weakened by magma. Such strain/magmatism feedback interactions are routinely described in actively deforming shear zones (Druguet et al., 2008; Butler and Torvela, 2018; Alsop et al., 2021).

The results above clearly show that theoretical models about syncontractional intrusive sheets (e.g., Hubbert and Willis, 1957; Sibson, 2003; Tibaldi, 2005; Gonzales et al., 2009) only apply to a moderate amount of WAS magma-filled fractures, i.e. those dipping shallowly or oriented parallel to the shortening direction. These are the only intrusions thought to have

been directly controlled by the ambient tectonic stresses. Conversely, two alternative driving forces, i.e. host-rock tectonic anisotropies (S_1 and D_3) and structural inheritance, likely operated during the emplacement of the prominent orogen-parallel WAS intrusion population. In such contexts, the mean orientation of most intrusive sheets does not pertain to a direct relation to the regional stress/strain field and thus cannot be used as a proxi for time-averaged stresses (Gudmundsson, 1995; Sato et al., 2013).

5.2. The WAS complex in the Armorican Variscan context

The Variscan orogeny in the Armorican massif was accompanied by a voluminous and relatively homogeneous magmatic cortege, dominated by massive granitoid intrusions. Most of them are parts of a synorogenic intrusive system formed in the time-range 320-305 Ma (Bernard-Griffith et al., 1985; Tartèse et al., 2011; Le Gall et al., 2014) along a composite crustal-scale dextral shear zone pattern comprising of the NASZ (Saint-Renan, Huelgoat, Commana/Plouaret granites) and the SASZ (Pontivy, Lizio, Questembert granites; Fig. 13b). Younger synkinematic granitic plutons were emplaced in three various structural contexts (Fig. 13b). At ca. 300 Ma, the Quintin granite intruded along the central part of the NASZ (Peucat et al., 1984), whereas the Aber-Ildut/Brignogan granite association (Marcoux et al., 2009) was emplaced during sinistral shearing along the N70°E-oriented Porspoder-Guisseny lineament in the LMD (Chauris, 1994). The kinematic change from dextral to sinistral shearing resulted from the clockwise rotation (from NW-SE to N-S) of the applied stress field (Rolet et al., 1986). A third group of granites (Carnac, Guérande, Quiberon, Sarzeau, in Fig. 13b) were emplaced during extensional tectonics in the time-span 310-300 Ma (Le Hebel et al., 2002; Turillot et al., 2011) and thus marked fundamental geodynamical changes related to the gravitational collapse of the chain in the South Armorican domain (Gapais et al. 1993; Cagnard et al., 2004).

From the brief review above, it thus appears that the only common structural feature displayed by the WAS complex and others Armorican Variscan magmatic intrusions is the inherited origin and collinear map-trace of its inferred feeder zone (Le Roz) with those of the Huelgoat granite (MASZ; Fig. 13). These deeply-rooted discontinuities acted, possibly diachronously, as pathways for lamprophyric and granitic magmas, in response to abrupt lateral heterogeneities at depth in the mantle during the Variscan events.

But, more generally, the WAS complex radically differs from the synorogenic Armorican magmatic systems with its specific lamprophyre-type nature. Another lamprophyric network occurs in the NW part of the LMD (Fig. 13b), but it is composed of leucominettes (Caroff et al., 2015) derived from very different compositionally products and further emplaced in a quite distinct structural context. Indeed, the leucominette swarm, genetically related to the ca. 300 Ma-old Aber-Ildut granite (Caroff et al., 2015), only comprises a few dykes, approximated to N-S tension-gashes formed parallel to the regional shortening axis (Rolet et al., 1986) during a late orogenic sinistral shearing event.

With regards to the Armorican Variscan framework, the WAS complex appears as the only lamprophyre intrusive sheet network intruded during the main shortening phase. Therefore, the nature of the causal mechanisms of such a magmatic and structural specificity should be questioned. Elements of answer are supplied from its restricted spatial distribution in the Brest syncline, with a preferred focus in the youngest (Middle/Upper Devonian) series coring its axial part (Figs. 2a, 13a). This is exemplified along the northern edge of the syncline where the Brioverian schist series occurring immediately north of the Elorn bounding shear zone, beyond the limits of the initial Paleozoic basin, are devoid of any intrusive sheets despite the proximity of the Caro potential feeder zone. The influence of a lithological/rheological contrast on magma distribution is excluded because: (i) Brioverian schists are a relatively weak material that should have rather helped magma injection, and (ii) these series are

necessarily intruded at depth underneath the Paleozoic succession filling the Brest syncline. One possible mechanism, illustrated on the lithospheric-scale sketch in Fig. 15, is based on the following evidence. Since highly-displaced allochthonous units are not present in the moderately-strained Brest syncline, the map distribution of WAS intrusions roughly coincides with the main Paleozoic sedimentary depocenter. Because of the lack of any Variscan crustal-scale thrust structures, the initial (basinal) lithosphere profile must have been preserved during the orogenic events. Consequently, the necking zone of the stretched lithosphere, inferred to still underlie the Paleozoic depocenter, may have later favored ponding of melting sources directly beneath the Brest syncline. This assumption agrees with the geobarometric results of Caroff et al. (2021) which indicate an anomalously shallow paleodepth of 80 ± 5 km for the melting sources of the kersantite magmas at the base of the lithosphere.

5.3. The WAS complex in the magmatic context of the European Variscides

Lamprophyre-type magmatism is common throughout the European Variscides, for instance in (Fig. 1a): (i) the South Bohemian massif (Zeitlhofer et al., 2014), (ii) the Black Forest (Hegner et al., 1998), (iii) the Western Swiss Alps (Monjoie et al., 2007; Filippi et al., 2019), and (iv) the Central Iberian Zone (Scarrow et al., 2011). Most of these complexes display a wide spectrum of magmatic affinities, typically indicative of both orogenic and anorogenic systems. They are generally related to wrench tectonics in either transpressional or transtensional settings (for review see Scarrow et al., 2011). The great variety of lamprophyric magmas injected at various stages of the Variscan orogeny is particularly well expressed in the SE Bohemian massif (Fig. 1b). Because most of the corresponding published works are mainly devoted to strictly magmatic (geochemical and radiometric) issues (for review see Krmicek et al., 2020), direct comparisons with the structural results obtained here about the WAS complex are made difficult. Nevertheless, correlations can be attempted between

successive generations of lamprophyre intrusions reported in both the NW Armorican and SE Bohemian segments, though significant differences exist in terms of temporal patterns and structural significance in the orogen history. In the Moldanubian zone (SE Bohemian massif, Figs. 1a, b), a hiatus of ca. 10 Ma. separates the emplacement of an early intrusive sheet network showing orogenic magmatic affinities (Neubauer et al., 2003; Kubinova et al., 2017), possibly comparable to the WAS complex, and younger lamprophyre intrusions typically displaying anorogenic affinities (Fig. 1c; Neubauer et al., 2003). By contrast, a continuum seems to exist in the NW Armorican lamprophyre system between the injection of the WAS complex during the main shortening event and the ca. 300 Ma-old leucominette dyke swarm in the LMD which still displays orogenic magmatic affinities (Caroff et al, 2015), in agreement with its emplacement in a sinistral transpressional setting at a later orogenic stage.

At a larger scale, the genetic links evoked above between the Variscan lamprophyre-type magmatism and strike-slip tectonics are also mentioned in the compiled work of Scarrow et al. (2011) about older orogens, Archaean (Canada) or Caledonian in age (E Ireland, NW England), as well as about younger Cenozoic orogens (NW China, Tibet, Balkans). These links have been variously interpreted and, for example, in the model proposed by Vaughan and Scarrow (2003) K-rich mantle-derived (low-degree) melts tend to promote focusing of strain along steep discontinuities prone to be subsequently reactivated as wrench shear zones, depending on the stress field. At a first order, this model should apply to the WAS complex, given the dextral shear zone nature of the Le Roz feeder zone, but with caution because of the role assigned to structural inheritance in our model.

6. Conclusions

- Our structural study is devoted to a lamprophyric sheet swarm cutting through low-grade and moderately-deformed Paleozoic metasedimentary host-rocks occurring in a

Variscan transpressional setting at the western termination of the Central Armorican Domain, western France.

- The so-called West Armorican Swarm (WAS) is composed of nearly 100 individual intrusive sheets (mostly kersantite), identified on a reference coastal cross-section, and analyzed in terms of geometry, propagation and timing of emplacement with respect to the strained host-rocks.

- Strain/intrusion mutual relationships indicate that magma injection took place during the regional shortening, *via* multiple pulses which alternated with three strain events (D_1, D_2, D_3).

- Most of individual sheets are: (i) <5 m in width, (ii) moderately- to steeply-inclined (90% >30°), and (iii) preferentially oriented N70-90°E, parallel to the trace of the regional S_1 cleavage, i.e. nearly normal to the direction of shortening.

- These structural features do not match with theoretical models. They are satisfactorily integrated in a tectonic model which favours the influence of both host-rock planar anisotropies (S_1 cleavage and D_3 shear structures) and structural inheritance on the propagation of magma in the WAS complex. The role of the ambient stress field is only hypothesized about a few WAS intrusions, parallel to the shortening direction.

- The WAS intrusions generally escaped deformation. Most of strained (boudinaged) intrusive sheets occur in an inferred magmatic feeder zone (Le Roz), further reactivated as a dextral shear zone.

- At the scale of the European Variscan belt, syncontractionnal lamprophyre complexes comparable to the WAS system are only reported in the SE Bohemian massif.

- Considering the WAS complex as a reference example for lamprophyre magmas emplaced in a shortened mid/upper crust requires the following conditions: (i) a subduction zone and associated mantle-derived melts, (ii) a previous long-lived and subsiding

sedimentary basin (with its thick pile of sediments) underlain by a lithospheric necking zone, still preserved during the orogenic stage, and which will later promote ponding of the melting material. The modest dimensions of the initial basin, mirrored at depth by those of the necking zone, accounts for the spatially-restricted distribution of the syncollisional magmatic products. Lastly, (iii) a steep network of crustal-scale discontinuities, subsequently recording dextral shearing in the present case (Variscan transpressional setting), act as propagation pathways (feeder zones) for the deep magma up to shallower crustal levels.

Declaration of Competing Interest

No competing interests.

Data availability

Data will be made available on request.

Acknowledgements

Funding of our work was mostly supplied by the Parc Naturel Regional Armorique in the framework of the (UNESCO) « Armorique Geopark" project conducted by Jérémie Bourdoulous and Noémie Courant who are warmly thanked. Our colleagues Jean-Alix Barrat, Christine Authemayou, Gilles Chazot and Laurent Geoffroy (Geo-Ocean, UMR 6538), as well as Mohamed Ahmed Daoud (CERD Djibouti), are acknowledged for fruitful discussions in the field. Dr. José Ramon Catalàn (Salamanca univ.) provided useful comments that have been appreciated. Kelly Cayocca (Troglogites Monts d'Arrée) is thanked for "polishing" the English form of parts of the text. We gratefully acknowledge Dr. S. Angiboust (Editor) and the reviewers M. Faure and one anonymous, with special thanks to D. Zanoni for his thorough examination of the paper and his constructive comments.

Supplementary data

Supplementary data to this article can be found online…

CRediT authorship contribution statement

Bernard Le Gall: Conceptualization, Methodology, Investigation, Writing, Visualization. Martial Caroff: Investigation, Formal analysis, Validation, Funding acquisition.

References

Alsop, G., Strachan, R., Holdsworth, R., Burns, I., 2021. Geometry of folded and boudinaged pegmatite veins emplaced within a strike-slip shear zone: a case study from the Caledonian orogen, northern Scotland. J. Struct. Geol. 142, 104233.

Anderson, E., 1951. The dynamics of faulting and dyke formation with applications to Britain. Oliver & Boyd, Edinburgh.

Authemayou, C., Le Gall, B., Caroff M., Bussien-Grosjean, D., 2019. Wrench- related dome formation and subsequent orogenic syntax bending in a hot orogen (Variscan Ibero-Armorican Arc, the Ouessant Island, France). Tectonics 38. https://dx.doi.org/10.1029/2018TC005189.

Babin, C., Darboux, J.R., Duée, G., Gravelle, M., Morzadec, P., Plusquellec, Y., Thonon, P., 1975. Tectoniques tangentielles et tectoniques superposées dans le Dévonien de la Rade de Brest. C. R. Acad., Sc., Paris 280, 259-262.

Babin, C., Darboux, J.R. (coordinators), 1982. Geological map of France, sheet Le Faou (275). BRGM, Orléans, scale 1:50,000.

Balé, P., Brun, J-.P., 1986. Les complexes métamorphiques du Léon (NW Brittany): un segment du domaine éohercynien sud-armoricain translaté au Dévonien. Bull. Soc. Geol. Fr. 8(2), 471-477.

Ballèvre, M., Bosse, V., Ducassou, C., Pitra, P., 2009. Paleozoic history of the Armorican Massif. Models for the tectonic evolution of the suture zones. C. R. Geosci. 341, 174-201.

Ballouard, C., 2016. Origine, évolution et exhumation des leucogranites peralumineux de la chaîne hercynienne armoricaine : implication sur la métallogénie de l'uranium. Ph.D. thesis. Rennes1 univ. France.

Bernard-Griffiths, J., Peucat, J., Sheppard, S., Vidal, P., 1985. Petrogenesis of Hercynian leucogranites from South Armorican massif. Contributions of REE and isotopic (Sr, Nd, Pb, O) geochemical data to the study of source rock characteristics and ages. Earth Planet. Sci. Lett. 74, 235-250.

Bertelsen, H., Rogers, B., Galland, O., Dumazer, G., Bennani, A., 2018. Laboratory modelling of coeval brittle and ductile deformation during magma emplacement into viscoelastic rocks. Front. Earth Sci. (https://doi.org/10.3389/feart.2018.00199.

Butler, R., Torvela, T., 2018. The competition between rates of deformation and solidification in synkinematic granitic intrusions: resolving the pegmatite paradox. J. Struct. Geol. 117, 1-13.

Cagnard, F., Gapais, D., Brun, J.-P., Gumiaux, C., van den Driessche, J., 2004. Late pervasive crustal-scale extension in the south Armorican Hercynian belt (Vendée, France). J. Struct. Geol. 26, 435-449.

Caroff, M., Barrat, J.-A., Le Gall, B., 2021. Kersantites and associated intrusives from the type locality (Kersanton), Variscan belt of Western Armorica (France). Gondwana Res. 98, 46-62.

Caroff, M., Labry, C., Le Gall, B., Authemayou, C., Bussien Grosjean, D., Guillong, M., 2015. Petrogenesis of late-Variscan high-K alkali-calcic granitoids and calc-alkalic

lamprophyres: The Aber-Ildut/North-Ouessant complex, Armorican Massif, France. Lithos 238, 140–155. http://dx.doi.org/10.1016/j.lithos.2015.09.025.

Caroff, M., Le Gall, B., Authemayou, C., 2020. How does a monzogranite turn into a trachydacitic extrusion mantled by basinal volcaniclastics and peperites? The case of South Ouessant, Armorican Variscides (France). J. Geol. Soc., London doi.org/10.1144/jgs2020-060.

Caroff, M., Le Gall, B., Authemayou, C., Bussien Grosjean, D., Labry, C., Guillong, M. 2016. Relations between basalts and adakite-felsic intrusive bodies in a soft-substrate environment: the South Ouessant Visean basin in the Variscan belt, Armorican Massif, France. Can. J. Earth Sci., 53, 441-456, https://doi.org/10.1139/cjes-2015-0230.

Castaing, C. et al., 1987. Geological map of France, sheet Huelgoat (276). BRGM, Orléans, scale 1: 50,000.

Chauris, L., 1994. Geological map of France, sheet Plouarzel/île d'Ouessant (295), BRGM, Orléans, scale 1: 50,000.

Chauris, L., Plusquellec, Y. et al., 1989. Geological map of France, sheet Brest (274). BRGM, Orléans, scale 1: 50,000.

Darboux, J.-R., Le Gall, B. 1988. Les Montagnes Noires : cisaillement bordier méridional du bassin carbonifère de Châteaulin (Massif Armoricain, France). Caractéristiques structurales et métamorphiques. Geodinamica Acta 2(3), 121-133.

Darboux, J.-R., Marcoux, E., Hallégouët, B., Lebret, P., Sorel, P., 2010. Geological map of France, sheet Landerneau (239). BRGM, Orléans, scale 1: 50,000.

Delaney, P., Pollard, D., Ziony, J., McKee, E., 1986. Field relations between dikes and joints: emplacement processes and paleostress analysis. J. Geophys. Res. Solid Earth 91 (B5), 4920-4938.

Doubinger, J., Pelhate, A., 1976. Nouvelles observations sur l'âge des schistes de Châteaulin (Massif armoricain). C. R. Acad. Sci., Paris 283, 467.

Druguet, E., Czeck, D., Carreras, J., Castano, L., 2008. Emplacement and deformation features of syntectonic leucocratic veins from Rainy Lake zone (Western Superior Province, Canada). Precambrian Res. 163 (3-4), 384-400.

Faure, M., Bé Mézème, E., Cocherie, A., Rossi, P., Chemenda, A., Boutelier, D., 2008. Devonian geodynamic evolution of the Variscan Belt, insights from the French Massif Central and Massif Armoricain. Tectonics 27, doi.org/10.1029/2007 TC002115.

Faure, M., Sommers, C., Melleton, J., Cocherie, A., Lautout, O., 2010. The Léon domain (French Massif armoricain): a westward extension of the Mid-German Crystalline Rise? Structural and geochronological insights. Int. J. Earth Sci. 99, 65-81.

Ferré, E., Galland, O., Montanari, D., Kalakay, T., 2012. Granite magma migration and emplacement along thrusts. Int. J. Earth Sci. 1-16. doi: 10.1007/s00531-012-0747-6.

Filippi, M., Zanoni, D., Gosso, G., Lardeaux, J.-M., Verati, C., Spalla, M.I., 2019. Structure of lamprophyres: a discriminant marker for Variscan and Alpine tectonics in the Argentera-Mercantour Massif, Maritime Alps. Bull. Soc. Géol. France 190, 1 https://doi.org/10.1051/bsgf/2019014

Foster, D., Schafer, C., Fanning, M., Hyndman, D., 2001. Relationships between crustal partial melting, plutonism, orogeny, and exhumation: Idaho-Bitterroot batholith, Tectonophysics 342, 313-350.

Galland, O., de Bremond d'Ars, J., Cobbold, P., Hallot, E., 2003. Physical models of magmatic intrusion during thrusting. Terra Nova 15, 405-409.

Galland, O., Cobbold, P., de Bremond d'Ars, J., Hallot, E., 2007a. Rise and emplacement of magma during horizontal shortening of the brittle crust: Insights from experimental modeling. J. Geophys. Res. 112, B06402, doi:10.1029/2006JB004604.

Galland, O., Hallot, E., Cobbold, P., Ruffet, G., de Bremond d'Ars, J., 2007b. Volcanism in a compressional Andean setting: A structural and geochronological study of Tromen volcano (Neuquén province, Argentina). Tectonics 26, TC4010, doi:10.1029/2006TC002011.

Gapais, D., Le Corre, C., 1980. Is the Hercynian belt of Brittany a major shear zone? Nature 288, 574-576.

Gapais, D., Lagarde, J., Le Corre, C., Audren, C., Jegouzo, P., Casas Sainz, A., van den Driessche, J., 1993. La zone de cisaillement de Quiberon : témoin d'extension de la chaîne varisque en Bretagne méridionale au Carbonifère. C. R. Acad. Sci., Paris 316, 1123-1129.

Glazner, A., 1991. Plutonism, oblique subduction, and continental growth: An example from the Mesozoic of California, Geology 19, 784-786.

Gonzalez, G., Cembrano, J., Aron, F., Veloso, E., Shyu, J., 2009. Coeval compressional deformation and volcanism in the central Andes, case studies from northern Chile (23°S-24°S). Tectonics 28, 6, TC6003.

Goulty, N., 2005. Emplacement mechanism of the Great Whin and Midland Valley dolerite sills. J. Geol., Soc., London 162, 1047-1056.

Gudmundsson, A., 1995. Infrastructure and mechanics of volcanic systems in Iceland. J. Volc. Geother. Res. 64/1-2, 1-22.

Gumiaux, C., Judenherc, S., Brun, J.-P., Gapais, D., Granet, M., Poupinet, G., 2004. Restoration of lithosphere-scale wrenching from integrated structural and tomographic data (Hercynian belt of western France). Geology 32, 333-336.

Hamilton, W., 1995. Subduction systems and magmatism. In: J., Smellie (ed.), Volcanism associated with extension at consuming plate margins. Geol. Soc. Lond., Spec. Pub. 3-28.

Hegner, E., Kolbl-Ebert, M., Loeschke, J., 1998. Post-collisional Variscan lamprophyres (Black Forest, Germany): $^{40}Ar/^{39}Ar$ phlogopite dating, Nd, Pb, Sr isotope, and trace element characteristics. Lithos 45, 395-411.

Hollister, L., Crawford, M., 1986. Melt-enhanced deformation: a major tectonic process. Geology 14, 558-561.

Hubbert, M., Willis, D., 1957. Mechanics of hydraulic fracturing. In: Hubbert, M., (ed), Structural Geology 175-190, Macmillan, New York.

Jones, K., 1994. Progressive metamorphism in a crustal-scale shear zone: an example from the Leon region, NW Brittany, France. J. Metam. Geol. 12, 69-88.

Kjøll, H., Andersen, T., Corfu, F., Labrousse, L., Tegner, C., Abdelmalak, M., Planke, S., 2019. Timing of break-up and thermal evolution of a pre-Caledonian Neoproterozoic exhumed magma-rich rifted margin. Tectonics doi.org/10.1029/2018TC005375.

Krmicek, L., Romer, R., Timmerman, M., Ulrych, J., Glodny, J., Prichystal, A., Sudo, M., 2020. Long-lasting (65 Ma) regionally contrasting late- to post-orogenic Variscan mantle-derived potassic magmatism in the Bohemian massif. J. Pet. Geol. 61, 7, doi: 10.1093/petrology/egaa072.

Kroner, U., Romer, R., 2013. Two plates - Many subduction zones: The Variscan orogeny reconsidered. Gondwana Res. 24, 298-329.

Kubinova, S., Faryad, S., Verner, K., Schmitz, M., Holub, F. 2017. Ultrapotassic dykes in the Moldanubian Zone and their significance for understanding of the post-collisional mantle dynamics during Variscan orogeny in the Bohemian Massif. Lithos 272-273, 205-221.

Le Gall, B., Authemayou, C., Ehrhold, A., Paquette, J.-L., Bussien, D., Chazot, G., et al., 2014. LiDAR offshore structural mapping and U/Pb zircon/monazite dating of Variscan strain in the Léon metamorphic domain, NW Brittany. Tectonophysics 630, 236-250. https://doi.org/10.1016/j.tecto.2014.05.026.

Le Gall, B., Authemayou, C., Graindorge, D., Duperret, A., Kaci, T., Ehrhold, A., Schmitt, T. 2021. Status of basement terranes in orogens : Insights from the Cadomian Domain of the North Armorican Variscides, Western France. Tectonics 40(5), doi : 10.1029/2020TC006578.

Le Gall, B., Loboziak, S., Le Herissé, A., 1992. Le flanc sud du synclinorium carbonifère de Châteaulin (Massif Armoricain, France) : une bordure de bassin reactivée en contexte decro-chevauchant. Bull., Soc., geol., Fr. 163, 1, 13-26.

Le Hebel, F., Vidal, O., Kienast, J., Gapais, D., 2002. Les porphyroïdes de Bretagne méridionale : une unité de HP-BT dans la chaîne hercynienne. C. R. Géosci. 334, 205-211.

Lister, J., Kerr, R., 1991. Fluid-mechanical models of crack propagation and their application to magma transport in dykes. J. Geophys. Res. 96, 10049-10077.

Marcoux, E., Cocherie, A., Ruffet, G., Darboux, J.-R., Guerrot, C., 2009. Géochronologie revisitée du dôme du Léon (Massif armoricain, France). Géol. Fr. 1, 19-40.

Mazzarini, F., Musumeci, G., Montanari, D., Corti, G., 2010. Relations between deformation and upper crustal magma emplacement in laboratory physical models. Tectonophysics 484, 13-146.

Menand, T., Daniels, K., Benghiat, P., 2010. Dyke propagation and sill formation in a compressive tectonic environment. J. Geophys. Res. 115, doi:10.1029/2009JB006791.

Meriaux, C., Lister, J., 2002. Calculation of dike trajectories from volcanic centers. J. Geophys. Res. 107, B4, doi:10.1029/2001JB000436.

Monjoie, P., Bussy, F., Schaltegger, U., Mulch, A., Lapierre, H., Pfeifer, H., 2007. Contrasting magma types and timing of intrusion in the Permian layered mafic complex of Mont Collon (western Alps, Valais, Switzerland): Evidence from U/Pb zircon and 40Ar/39Ar amphibole dating. Swiss J. Geosci. 100, 125-135.

Montanari, D., Corti, G., Sani, F., Del Ventisette, C., Bonini, M., Moratti, G., 2010a. Experimental investigation on granite emplacement during shortening. Tectonophysics 484, 1-4, 147-155.

Montanari, D., Corti, G., Simakin, A., 2010b. Magma chambers and localization of deformation during thrusting. Terra Nova 22, 390-395.

Neubauer, F., Dallmeyer, D., Fritz, H., 2003. Chronological constraints of late-and post-orogenic emplacement of lamprophyre dykes in the southeastern Bohemian Massif, Austria. Swiss Bull. Mineral. Petrol. 83, 317-330.

Paradis, S., Velde, B., Nicot, E., 1983. Chloritoid-pyrophyllite-rectorite facies rocks from Brittany, France. Contrib. Min. Pet. 83, 342-347.

Pasquare, F., Tibaldi, A., 2007. Structure of a sheet-laccolith system revealing the interplay between tectonic and magma stresses at Stardalur Volcano, Iceland. J. Volc. Geotherm. Res. 161, 131-150.

Peucat, J.-J., Auvray B., Hirbec Y., Calvez J.-Y., 1984. Granites et cisaillements hercyniens dans le Nord du Massif Armoricain : géochronologie Rb-Sr, Bull. Soc. géol. France 7, 26, 6, 1365-1373.

Plusquellec, Y., Rolet, J., Darboux, J.-R. et al., 1999. Geological map of France, sheet Châteaulin (310). BRGM, Orléans, scale 1: 50,000.

Pons, J., Barbey, P., Dupuis, D., Leger, J., 1995. Mechanisms of pluton emplacement and structural evolution of a 2.1 Ga juvenile continental crust: the Birimian of southwestern Niger. Precambrian Res. 70, 281-301.

Rolet, J., Thonon, P., 1978. La semelle d'un charriage hercynien majeur effondrée par un réseau de fractures en régime coulissant dextre : sa mise en évidence grâce aux marqueurs filoniens de la Rade de Brest (Massif armoricain). C. R. Acad. Sci., Paris 287, 1099-1102.

Rolet, J., Le Gall, B., Darboux, J.-R., Thonon, P., Gravelle, M., 1986. L'évolution géodynamique dévono-carbonifère de l'extrémité occidentale de la chaîne hercynienne d'Europe sur le transect Armorique-Cornwall. Bull. Soc. Geol. Fr. 8 (2), 43-54.

Scarrow, J., Molina, J., Bea, F., Montero, P., Vaughan, A., 2011. Lamprophyre dikes as markers of late orogenic transtension timing and kinematics: a case study from the Central Iberian Zone. Tectonics 30, doi:10.1029/2010TC002755.

Sato K, Yamaji, A., Tonai, S., 2013. Parametric and non-parametric statistical approaches to the determination of paleostress from dilatant fractures: application to an Early Miocene dike swarm in central Japan. Tectonophysics 588, 69-81.

Schofield, N., Brown, D., Magee, C., Stevenson, C. 2012. Sill morphology and comparison of brittle and non-brittle emplacement mechanisms. J. Geol. Soc., London 169, 127-141.

Schulz, B., 2013. Monazite EMP-Th-U/Pb age pattern in Variscan metamorphic units in the Armorican Massif (Brittany, France). German J. Geosci. 164, 313-335.

Sibson, R., 2003. Brittle-failure controls on maximum sustainable overpressure in different tectonic regimes. Am. Assoc. Petrol. Geol. Bull. 87(6), 901-908.

Takada, A., 1988. Subvolcanic structure of the central dike swarm associated with the ring complexes in the Shitara district, central Japon. Bull. Volc. 50, 106-118.

Tartèse, R., Boulvais, P., Poujol, M., Chevalier, T., Paquette, J.-L., Ireland, T., Deloule, E., 2011. Mylonites of the South Armorican Shear Zone: Insights for crustal-scale flow and water-rock interaction processes. J. Geodyn. doi:10.1016/j.jog.2011.05.003.

Tibaldi, A., 2005. Volcanism in compressional tectonic settings: Is it possible? Geophys. Res. Lett. 32, doi:10.1029/2004GL021798.

Tibaldi, A., Bonali, F., Corazzato, C., 2017. Structural control on volcanoes and magma paths from local- to orogen-scale: The central Andes case. Tectonophysics 699, 16-41.

Thonon, P., Rolet, J., 1982. Magmatisme et tectonique en Domaine Centre Armoricain occidental (Finistère). 107 Cong. Nat. Soc. Sav., Brest 355-366.

Turrillot, P., Augier, R., Monié, P., Faure, M., 2011. Late orogenic exhumation of the Variscan high-grade units (South Armorican Domain, western France), combined structural and $^{40}Ar/^{39}Ar$ constraints. Tectonics 30, http://dx.doi.org/10.1029/2010TC002788.

van Noorden, M., Sintubin, M., Darboux, J.-R., 2007. Strain partitioning in a slate belt: Evidence from the early Variscan Monts d'Arrée slate belt (Brittany, France). J. Struct. Geol 29, 837-849.

Vaughan, A., Scarrow, J., 2003. K-rich mantle metasomatism control of localization and initiation of lithospheric strike-slip faulting. Terra Nova 15, 163-169.

von Raumer, J., Finger, F., Veselá, P., Stampfli, G., 2014. Durbachites-Vaugnerites - a geodynamic marker in the central European Variscan orogen. Terra Nova 26, 85-95.

Walker, G., 1999. Volcanic rift zones and their intrusion swarms. J. Volc. Geotherm. Res. 94, 21-34.

Watanabe, T., Koyaguchi, T., Seno, T., 1999. Tectonic stress controls on ascent and emplacement of magmas. J. Volc. Geotherm. Res. 91, 65-78.

Watanabe, T., Masuyama, T., Nagaoka, K., Tahara, T., 2002. Analog experiments on magma-filled cracks: competition between external stresses and internal pressure, Earth Planets Space 54, 1247-1261.

Zeitlhofer, H., Schneider, D., Grasemann, B., Konstantin, P., Thöni, M., 2014. Polyphase tectonics and late Variscan extension in Austria (Moldanubian Zone, Strudengau area). Int. J. Earth Sc. 103, 83-102.

Zeitlhofer, H., Grasemann, B., Petrakakis, K., 2016. Variscan potassic magmatism of durbachitic affinity at the southern end of the Bohemian Massif (Lower Austria). Int. J. Earth Sc. 105, 1175-1197.

Captions

Fig. 1. *(2 columns)*

Geological setting. (a). The Armorican massif in a sketch map of the European Variscides, location of Figs. 1b and 1d. (b) Simplified magmatic map of the Bohemian massif showing the widespread distribution of lamprophyric complexes, modified from Krmicek et al. (2020). (c). Initial εNd/age diagram showing the orogenic *vs* anorogenic origin of the lamprophyric magmatism in the Bohemian and Armorican Variscan massifs, modified from Krmicek et al. (2020). (d) The main structural domains in the Armorican Variscides, Western France. CAD., Centre Armorican domain; CS., Châteaulin syncline; ESZ., MASZ., MNSZ., NASZ., SASZ., Elorn, Monts d'Arrée, Montagnes Noires, North Armorican, South Armorican shear zone, respectively; LMD., Leon metamorphic domain, SAD., South Armorican domain. The N70°-oriented LMD dome structure is not drawn. (e). Schematic structural cross-section at the transition from: (i) medium/high-grade metamorphic rocks in the southern flank of the LMD dome and (ii) low-grade metamorphic rocks in the WCAD. The continuity of the tectonic and metamorphic patterns is only disrupted by a network of discrete dextral shear zones (explanations and corresponding references in the text). ESZ, NASZ and PSZ., Elorn, North Armorican and Pierres Noires shear zones, respectively, location in Fig. 1d.

Fig. 2. *(2 columns)*

Structural sketch map of the Brest syncline. Intrusions are shown as point-like features, from 1: 50 000 geological maps (references in the text). C., Château headland; Ca., Caro; ESZ., Elorn shear zone; FT., transverse fault; G. Gluziau; I., Illien; IL., Ile Longue; K., Kerascoet; L., Larmor; LRSZ., Le Roz shear zone; NASZ., North Armorican shear zone; P., Porsguen. RT., Rozegat thrust, location in Fig. 1d. (b). Lithostratigraphy of the metasedimentary formations in the Brest syncline. (c). Structural cross-section in the Brest syncline. Specific stratigraphic formations are drawn as structural markers. Their stratigraphic position is shown in Fig. 2b. The WAS intrusive sheets, as well as the structures at depth, are not drawn.

Fig. 3. *(2 columns)*

Variscan ductile strain recorded by Paleozoic metasedimentary rocks in the Brest syncline. (a). An overturned syncleavage fold (D_1) in calcareous alternations (Le Faou Fm., stratigraphic position in Fig. 2b) exposed along the Larmor section (S_0, bedding; S_1, cleavage; location in Figs. 2a, c). (b). Stereographic diagram of the strike of the S_1 cleavage in the Northern unit (in %). (c). An overturned syncleavage fold (D_1) in the Southern unit (Traonliors Fm., stratigraphic position in Fig. 2b). Porsguen area; location in Figs. 2a, c. (d). Stereographic diagrams of the S_1 cleavage orientation in the Southern unit (equal area, lower hemisphere, Wulff projection). (d1). Poles to S_1 cleavage. (d2). Density contours of poles to S_1 cleavage. The best-fit great circle (dashed line) drawn by the contoured areas demonstrates folding of the S_1 cleavage by a second generation of fold (D_2) displaying a mean B_2 axis plunging 30° to N240°E. (e). Stereographic diagram of the strike of the S_1 cleavage planes in the Southern unit (in %). (f). A shallowly-dipping shear (thrust) structure cutting through folded schist series in the Southern unit. Kerarziou section; location in Fig. 2a, Supplementary Material Table S1).

Fig. 4. *(2 columns)*

Spatial distribution, orientation and width of the WAS intrusion network. (a). Histogram showing the amount of intrusions *per* km on the 20 km-long reference cross-section. (b, c, d). Stereographic diagrams of the intrusion strike for the total population (b), in the Northern unit (c) and in the Southern unit (d). The results are shown as %. (e). Histogram showing frequency-distributions of dip angles for all the intrusive sheets measured in the WAS. (f). Histogram showing frequency-distributions of widths for all the intrusive sheets measured in the WAS (see Supplementary Material Table S1).

Fig. 5. *(2 columns)*

Remarkable intrusive patterns in the WAS magmatic complex. (a). Kersantite ring-sheet structures observed in the South Château site. Note that the trace of the S_1 cleavage follows the margins of (i) the elliptical ring-sheets and (ii) the submeridian intrusions further east. (b, c). Transition patterns between steeply- and shallowly-inclined intrusion sheets in the South Château (b) and Caro (c) sites, location in Fig. 2a.

Fig. 6. *(2 columns)*

Main tectonic and magmatic structures in the Le Roz dextral shear zone. (a). Structural map showing: (i) two contrasted packages juxtaposed along an (inferred) thrust structure, and (ii) the intricate and lense-shaped geometry of most kersantite sheets in the lower (footwall) package. (b). Along-strike section showing a shallow microgranodiorite SIS thrusted over Upper Devonian schist series enclosing remnants of a kersantite sheet. (c). Structural cross-section through the highly-strained schist series (lower package) and its closely-spaced kersantite sheet network. (d). A moderately-inclined kersantite sheet (K_{63}) totally embedded in highly-sheared schists, but still displaying a well-preserved cooling joint pattern. Hammer (encircled) for scale. (e). Blocks of kersantite in a tectonic schist breccia. Hammer (encircled) for scale, location in Fig. 6c. See Supplementary Material Table S1.

Fig. 7. *(2 columns)*

Main tectonic and magmatic structures in the Ile Longue shear zone. (a). Sketch structural map showing two tectonic packages juxtaposed along a top-to-the-SW shear thrust contact, modified from Chauris et al. (1980). (b). Detailed structural map of the lower package showing the dismembered geometry of microgranodiorite sheets in a dextral ductile shear zone. (c). Cross-section showing the structural contrast between the two superposed packages. Trace of the section in Fig. 7a, completed and modified from Thonon and Rolet (1982).

Fig. 8. *(1.5 column)*

Relative chronology of strain and magmatic events in the Brest syncline. (a) Conceptual model illustrating the various ways host-rocks anisotropies have controlled the trajectory of magma in the WAS (Variscan) complex. No scale. See text for explanations. (b) Various intrusion networks alternating with three strain events (D_1, D_2, D_3). Kersantite and microgranodiorite undifferentiated). Black and white arrows correspond to fully and partly bracketed intrusive sheet populations, respectively. See Supplementary Material Table S1.

Fig. 9. *(2 columns)*

Tectonic and magmatic structures in the Château headland site, location in Fig. 2a. (a). Structural map showing two generations of kersantite sheets intruding Late Devonian schist series (Traonliors Fm.). (b). Structural cross-section illustrating two kersantite sheets dipping parallel with the S_1 cleavage, in a steep (HIS K_{51}) or shallow (SIS K_{53}) attitude. The SIS K_{53} is assumed to post-date both the D_2 fold structure and the HIS K_{51} in the lower package.

Fig. 10. *(2 columns)*

Various types of temporal relationships between strain and magma emplacement. (a). Detailed map of D_2 folds (schists/sandstones alternations in the Troaon Group) disrupted (post-dated) by three moderately-inclined kersantite sheets ($K_{82\text{-}84}$). Yelen site. (b). A thick microgranodiorite sheet (μGD_{33}) post-dated the D_1 event (S_1 enclaves) and is involved in (and pre-dated by) a top-to-the-SE thrust structure (D_3). Squiffiec site. (c). A 3 m-thick kersantite sheet (K_{23}) injected along a shallowly-inclined thrust fault cutting through steeply-dipping quartzitic strata (D_1 fold) of the Landevennec Fm. (d). Zoomed view showing an apophysis of the main sheet (upper margin) locally disrupted by shear surfaces. Intrusion drawn in blue, hammer (encircled) for scale. Larmor site, location in Fig. 2a.

Fig. 11. *(1 column)*

Structural evidence illustrating the emplacement of WAC intrusive sheets during shortening. (a, b). A shallowly-inclined kersantite sheet (K_{87}) in the Kerascoet site, (a) involved in (and pre-dating) a top-to-the-north (D_3) shear thrust and (b) enclosing a schist enclave (S_1) and thus post-dating the main ductile strain event (D_1), location in Fig. 2a. (c) Folded magmatic layering in a thin microgranodiorite sheet (μGD_{17}) injected along a top-to-the-NW shear thrust (D_3). Caro section, location in Figs. 2a, 5c. These timing constraints are consistent with those applied to the kersantite sheet K_{82} (Larmor section) and the microgranodiorite μGD_{33} (Squifiec section), location in Fig. 10.

Fig. 12. *(1 column)*

Structural evidence supporting the rigid/brittle mechanical behavior of the magmatic (sheets) and host-rock material during shortening. (a). A crack/fracture network formed by brittle failure of the schist host-rocks (Le Faou Fm.) ahead of a kersantite propagating tip (K_{24}). Hammer for scale. Larmor site. (b). A kersantite HIS, associated to the ring-sheet complex in the South Château site (K_{56}), displaying a wedge-shaped tip in Upper Devonian schist host-rocks (Porsguen Fm.). Hammer for scale. (c). Narrow shear zones (top-to-the-east and post-dating the intrusion emplacement) along the margins of a kersantite SIS (K_5). Note the still preserved vertical cooling joint pattern. Hammer for scale. Ilien ar Gwen site, location in Fig. 2a, and Supplementary Material Fig. S1.

Fig. 13. *(*2 columns)

The WAS lamprophyric complex in the Armorican Variscan framework. (a). Sketch structural map showing: (i) the contrasted strain regimes in the LMD and WCAD (decoupling and strain partitioning mechanisms are inferred) and (ii) the main magmatic features in the WAS complex (see text for explanations). The map-trace of WAS intrusions is only indicative with the aim to illustrate their parallelism (for most of them) with the regional cleavage (S_1). Spacing of the purple lines (intrusions) roughly reflects the density of the point-like features in the map in Fig. 2a. Same abbreviations as in Fig. 2a. (b) Spatial distribution of Variscan magmatic rocks in the Armorican belt. AI., Aber-Ildut; B., Brignogan; BS., Brest syncline; Ca., Carnac; CAD., Centre Armorican Domain; Co., Commana; G., Guérande; H., Huelgoat; LMD., Leon metamorphic domain; Pm., Ploumanac'h; Po., Pontivy; Q., Quintin; S., Sarzeau; SR., Saint-Renan; ESZ., MASZ., MNSZ., NASZ., PGSZ., SASZ., Elorn, Monts d'Arrée, Montagnes Noires, North Armorican, Porspoder-Guissény, South Armorican shear zones, respectively.

Fig. 14. *(2 columns)*

Dip intrusion distribution plotted against strikes. The two grey zones correspond to intrusive sheets that contradict theoretical models in terms of: (i) high (HIS) to moderate (MIS) dipping attitudes (dark grey) and (ii) orientation with respect to the direction of the regional shortening (Z) (light grey).

Fig. 15. *(2 columns)*

The WAS magmatic system in the lithospheric framework of the West Central Armorican Domain. The paleodepths of the crustal magmatic chamber and the melting sources in the necking lithosphere zone are from Caroff et al. (2021). The dashed line has no geological meaning (base of the section). CF., Caro feeder zone; LRF., Le Roz feeder zone. Others abbreviations as in Fig. 2a.

Supplementary Material

Table S1.

Fig. S1.

CRediT authorship contribution statement

Bernard Le Gall: Conceptualization, Methodology, Investigation, Writing, Visualization. Martial Caroff: Investigation, Formal analysis, Validation, Funding acquisition.

Declaration of Competing Interest

No competing interests.

- Structural analysis of a lamprophyre swarm cutting through strained host-rocks
- Magma injected during shortening in a Variscan transpressional setting, West France
- The role of host-rock planar anisotropies on magma pathway is emphasized
- Elaboration of a kinematic model about magma emplacement through a contracted crust

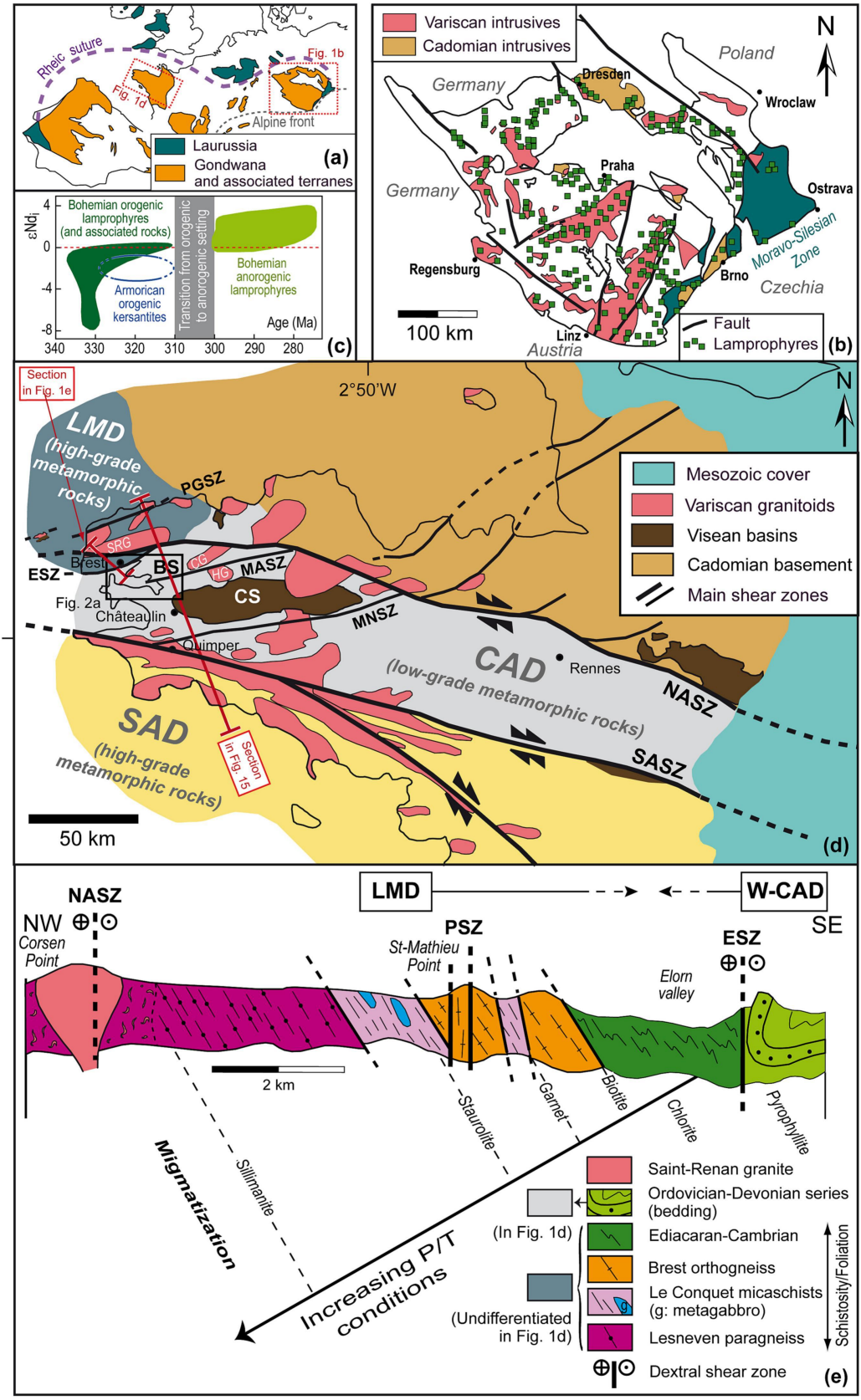
Rheic suture
Fig. 1b
Fig. 1d
Alpine front
Laurussia
Gondwana
and associated terranes
(a)
εNdi
Bohemian orogenic lamprophyres (and associated rocks)
Armorican orogenic kersantites
Transition from orogenic to anorogenic setting
Bohemian anorogenic lamprophyres
Age (Ma)
(c)
Variscan intrusives
Cadomian intrusives
N
Poland
Germany
Dresden
Wroclaw
Praha
Ostrava
Regensburg
Brno
Moravo-Silesian Zone
Czechia
Linz
Austria
100 km
Fault
Lamprophyres
(b)
Section in Fig. 1e
2°50'W
N
LMD (high-grade metamorphic rocks)
PGSZ
SRG
Brest
ESZ
BS
CC
HG
MASZ
CS
Fig. 2a
Châteaulin
MNSZ
Quimper
CAD
(low-grade metamorphic rocks)
Rennes
NASZ
SASZ
SAD
(high-grade metamorphic rocks)
Section in Fig. 1f
50 km
Mesozoic cover
Variscan granitoids
Visean basins
Cadomian basement
Main shear zones
48°00'N
(d)
NASZ
LMD
W-CAD
NW
SE
Corsen Point
PSZ
St-Mathieu Point
ESZ
Elorn valley
2 km
Staurolite
Garnet
Biotite
Chlorite
Pyrophyllite
Sillimanite
Migmatization
Increasing P/T conditions
Saint-Renan granite
Ordovician-Devonian series (bedding)
(In Fig. 1d)
Ediacaran-Cambrian
Brest orthogneiss
Le Conquet micaschists (g: metagabbro)
(Undifferentiated in Fig. 1d)
Lesneven paragneiss
Schistosity/Foliation
Dextral shear zone
(e)

Figure 1

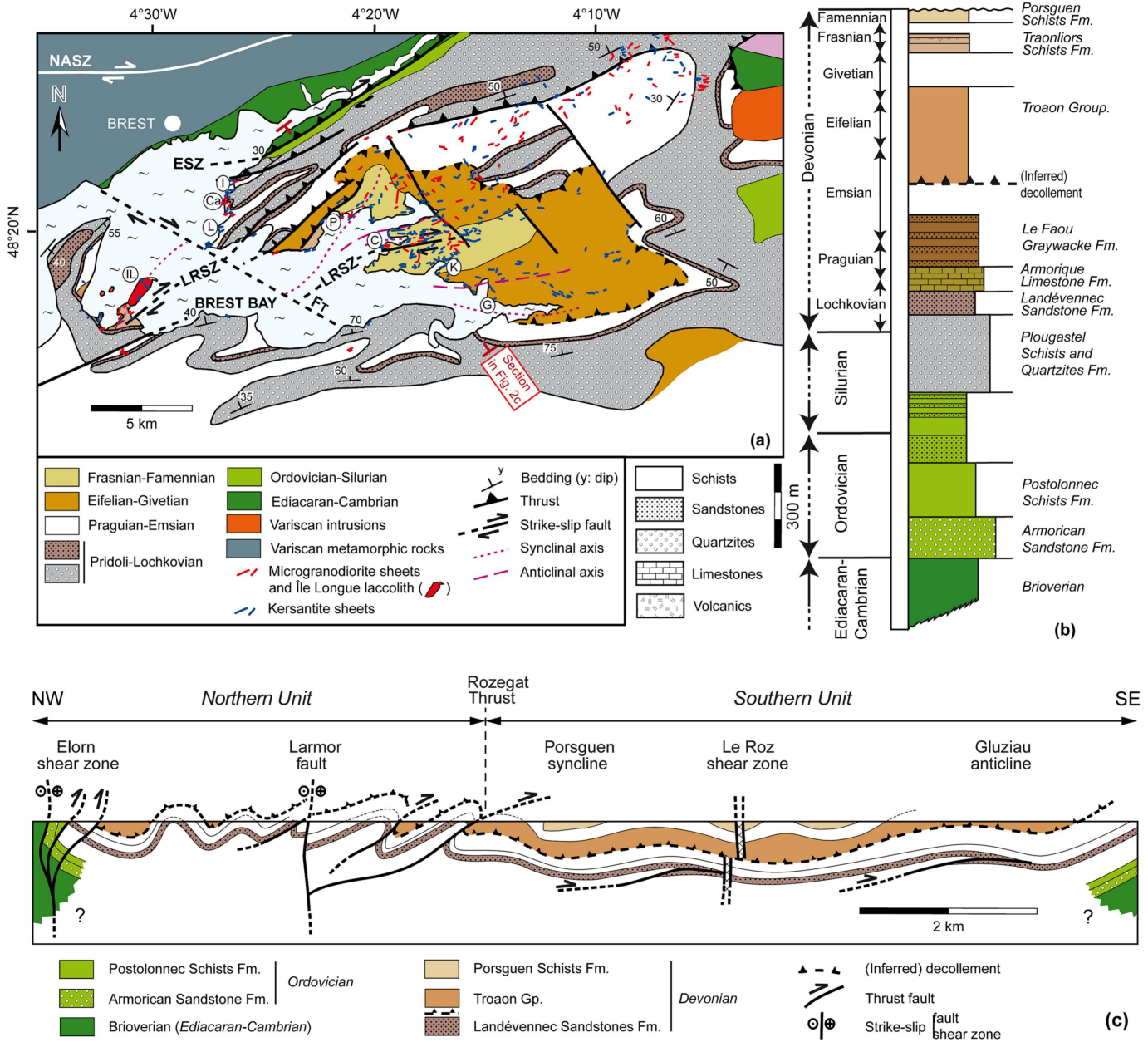
4°30'W
4°20'W
4°10'W
48°20'N
NASZ
N
BREST
ESZ
LRSZ
LRSZ
BREST BAY
Ft
I
Ca
L
P
C
K
G
IL
5 km
(a)
Section in Fig. 2c
Frasnian-Famennian
Eifelian-Givetian
Praguian-Emsian
Pridoli-Lochkovian
Ordovician-Silurian
Ediacaran-Cambrian
Variscan intrusions
Variscan metamorphic rocks
Microgranodiorite sheets and Île Longue laccolith
Kersantite sheets
Bedding (y: dip)
Thrust
Strike-slip fault
Synclinal axis
Anticlinal axis
Schists
Sandstones
Quartzites
Limestones
Volcanics
300 m
Famennian
Frasnian
Givetian
Eifelian
Emsian
Praguian
Lochkovian
Devonian
Silurian
Ordovician
Ediacaran-Cambrian
Porsguen Schists Fm.
Traonliors Schists Fm.
Troaon Group.
(Inferred) decollement
Le Faou Graywacke Fm.
Armorique Limestone Fm.
Landévennec Sandstone Fm.
Plougastel Schists and Quartzites Fm.
Postolonnec Schists Fm.
Armorican Sandstone Fm.
Brioverian
(b)
NW
Northern Unit
Rozegat Thrust
Southern Unit
SE
Elorn shear zone
Larmor fault
Porsguen syncline
Le Roz shear zone
Gluziau anticline
2 km
Postolonnec Schists Fm.
Armorican Sandstone Fm.
Brioverian (Ediacaran-Cambrian)
Ordovician
Porsguen Schists Fm.
Troaon Gp.
Landévennec Sandstones Fm.
Devonian
(Inferred) decollement
Thrust fault
Strike-slip fault
shear zone
(c)

Figure 2

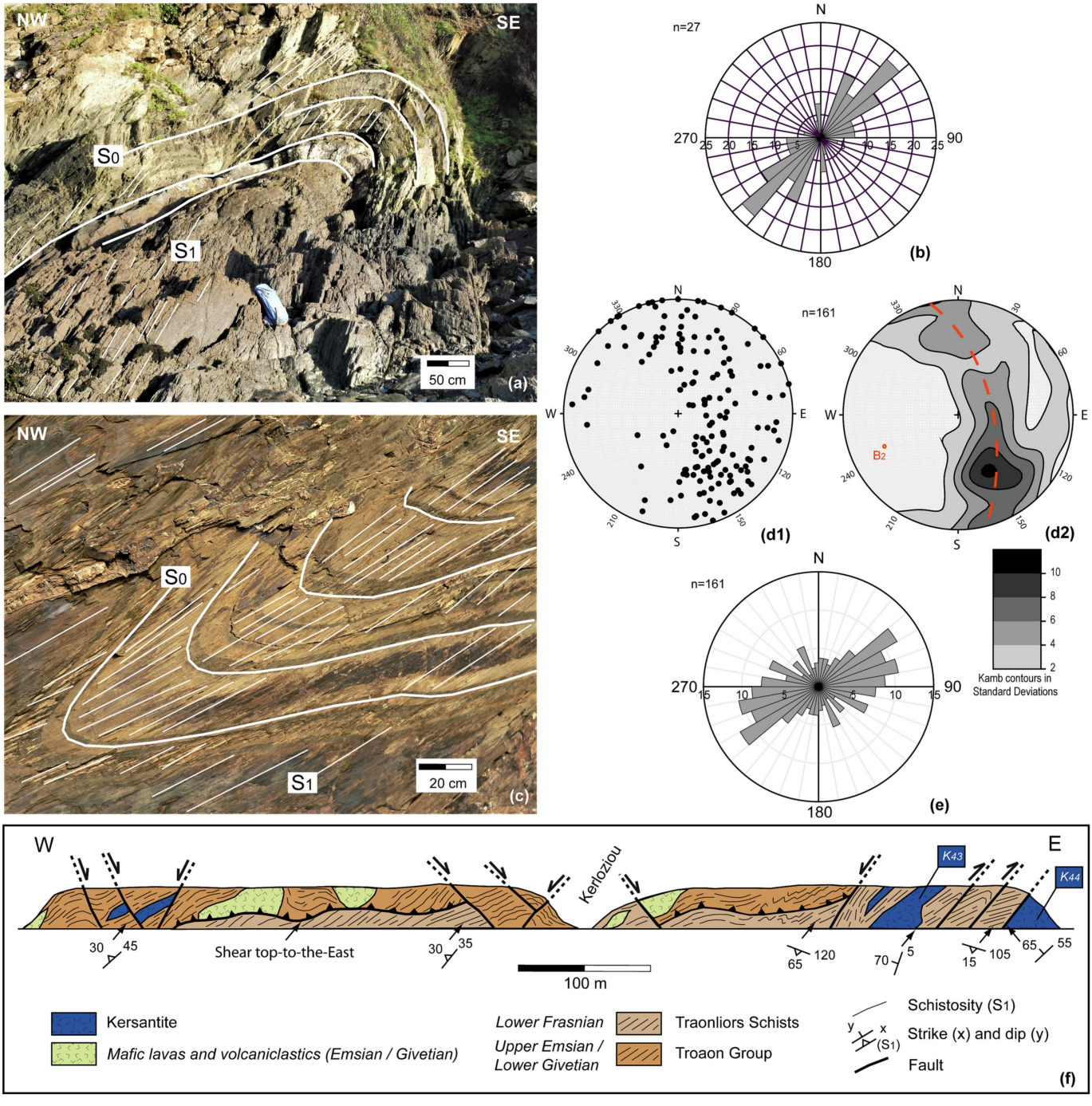
NW
SE
S0
S1
50 cm
(a)
n=27
N
90
180
270
(b)
n=161
(d1)
(d2)
B2
n=161
(e)
Kamb contours in Standard Deviations
NW
SE
S0
S1
20 cm
(c)
W
E
Kerloziou
K43
K44
30 45
Shear top-to-the-East
30 35
65 120
70 5
15 105
65 55
100 m
Kersantite
Mafic lavas and volcaniclastics (Emsian / Givetian)
Lower Frasnian
Upper Emsian / Lower Givetian
Traonliors Schists
Troaon Group
Schistosity (S1)
Strike (x) and dip (y)
Fault
(f)

Figure 3

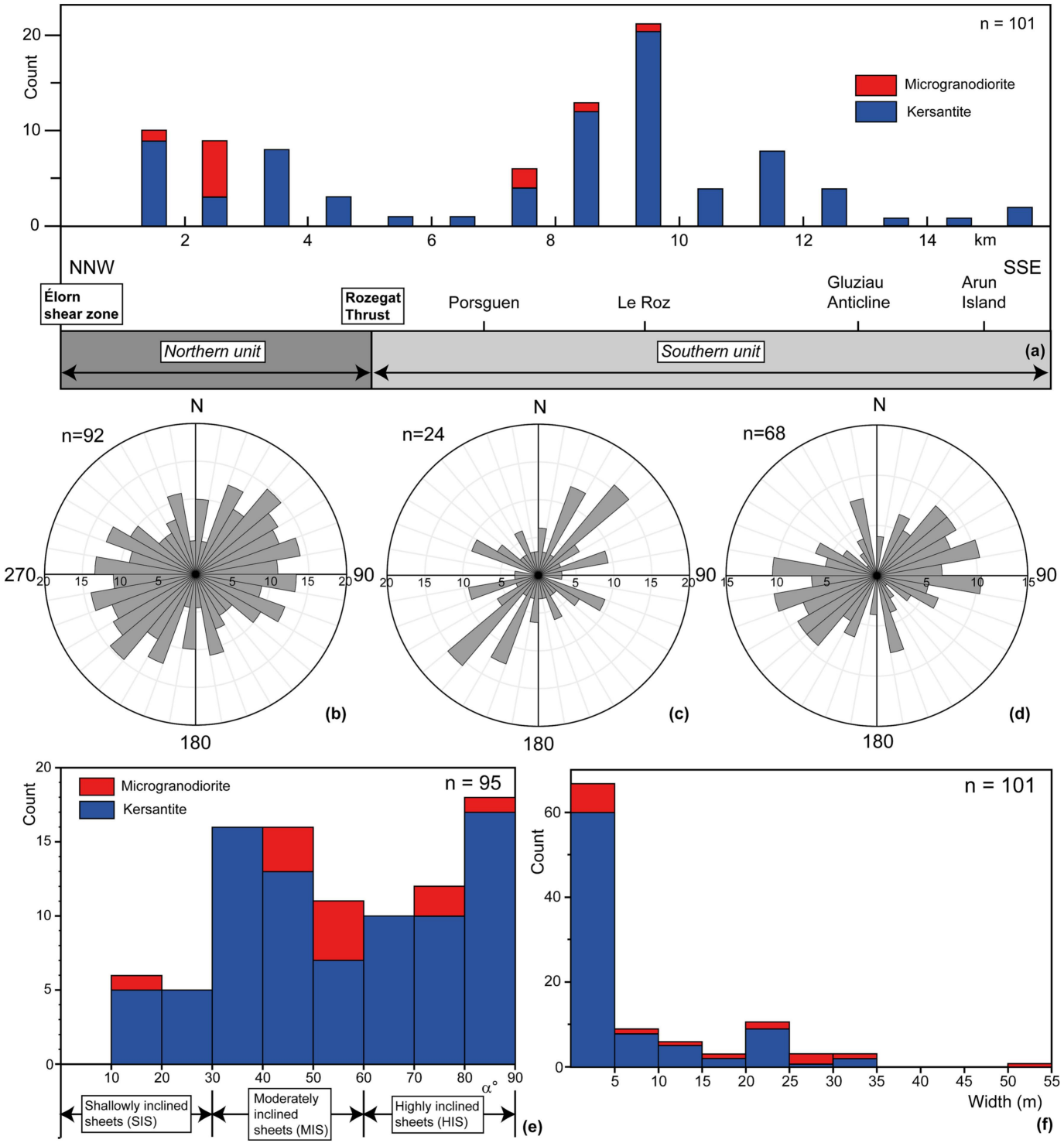
n = 101
Count
Microgranodiorite
Kersantite
km
NNW
SSE
Élorn shear zone
Rozegat Thrust
Porsguen
Le Roz
Gluziau Anticline
Arun Island
Northern unit
Southern unit
(a)
N
n=92
n=24
n=68
(b)
(c)
(d)
n = 95
α°
Shallowly inclined sheets (SIS)
Moderately inclined sheets (MIS)
Highly inclined sheets (HIS)
(e)
n = 101
Width (m)
(f)

Figure 4

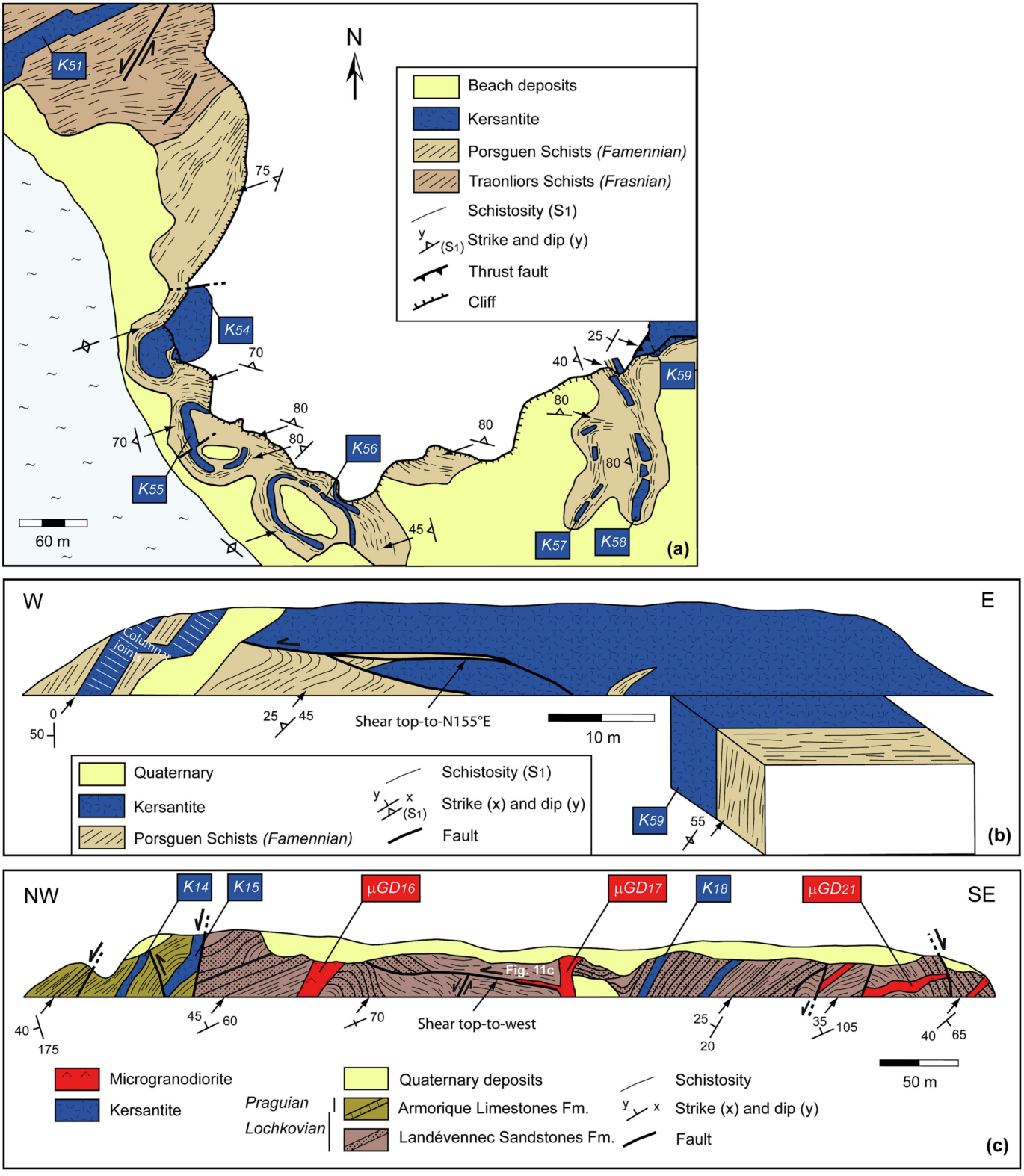
N
Beach deposits
Kersantite
Porsguen Schists (Famennian)
Traonliors Schists (Frasnian)
Schistosity (S1)
Strike and dip (y)
Thrust fault
Cliff
K51
K54
K55
K56
K57
K58
K59
60 m
(a)
W
E
Columnar joints
Shear top-to-N155°E
10 m
Quaternary
Kersantite
Porsguen Schists (Famennian)
Schistosity (S1)
Strike (x) and dip (y)
Fault
(b)
NW
SE
K14
K15
µGD16
µGD17
K18
µGD21
Fig. 11c
Shear top-to-west
50 m
Microgranodiorite
Kersantite
Praguian
Lochkovian
Quaternary deposits
Armorique Limestones Fm.
Landévennec Sandstones Fm.
Schistosity
Strike (x) and dip (y)
Fault
(c)

Figure 5

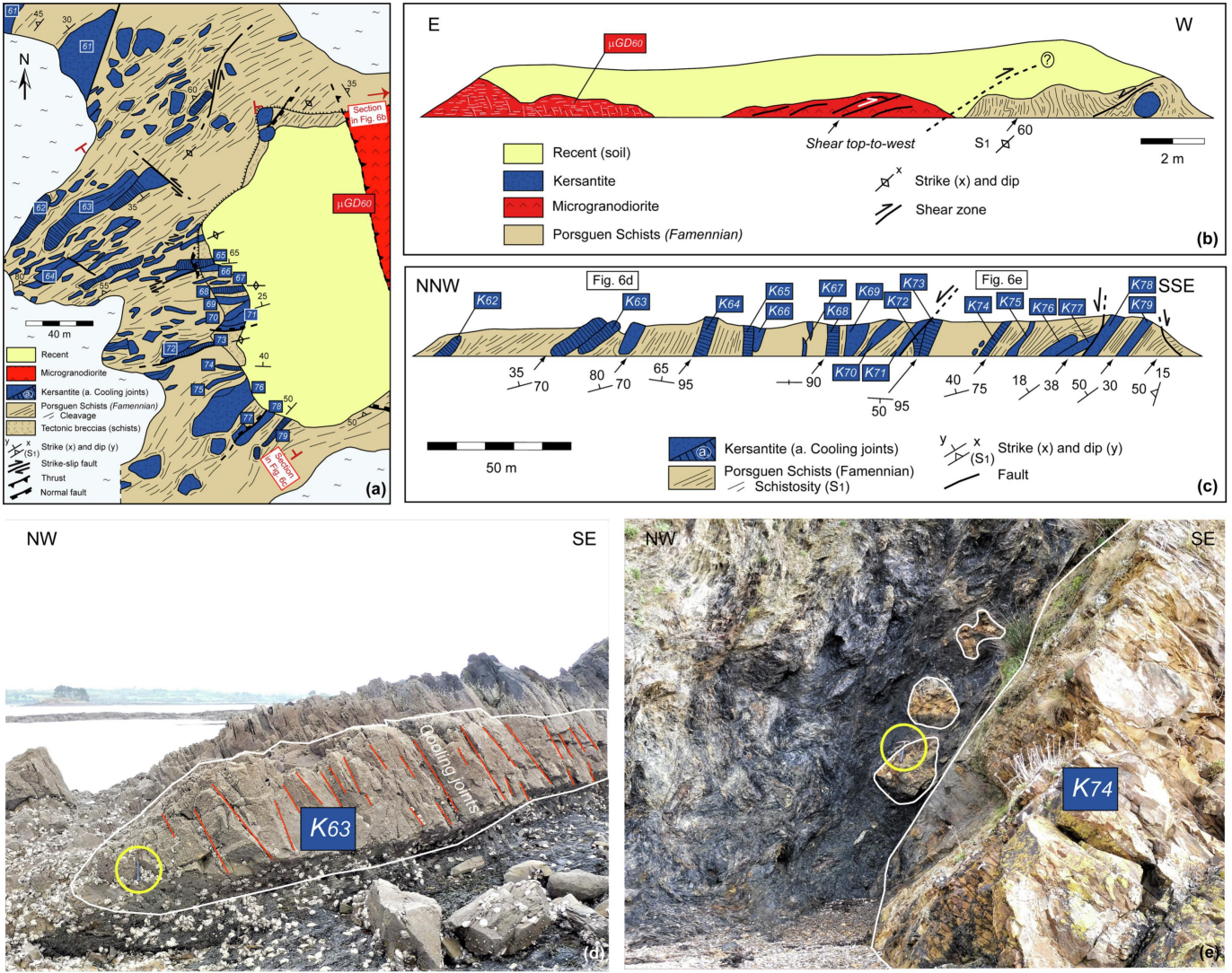
N
Section in Fig. 6b
μGD60
40 m
Recent
Microgranodiorite
Kersantite (a. Cooling joints)
Porsguen Schists (Famennian)
Cleavage
Tectonic breccias (schists)
Strike (x) and dip (y)
Strike-slip fault
Thrust
Normal fault
(a)
E
W
μGD60
Shear top-to-west
S1
2 m
Recent (soil)
Kersantite
Microgranodiorite
Porsguen Schists (Famennian)
Strike (x) and dip
Shear zone
(b)
NNW
SSE
Fig. 6d
Fig. 6e
50 m
Kersantite (a. Cooling joints)
Porsguen Schists (Famennian)
Schistosity (S1)
Strike (x) and dip (y)
Fault
(c)
NW
SE
K63
Cooling joints
(d)
NW
SE
K74
(e)

Figure 6

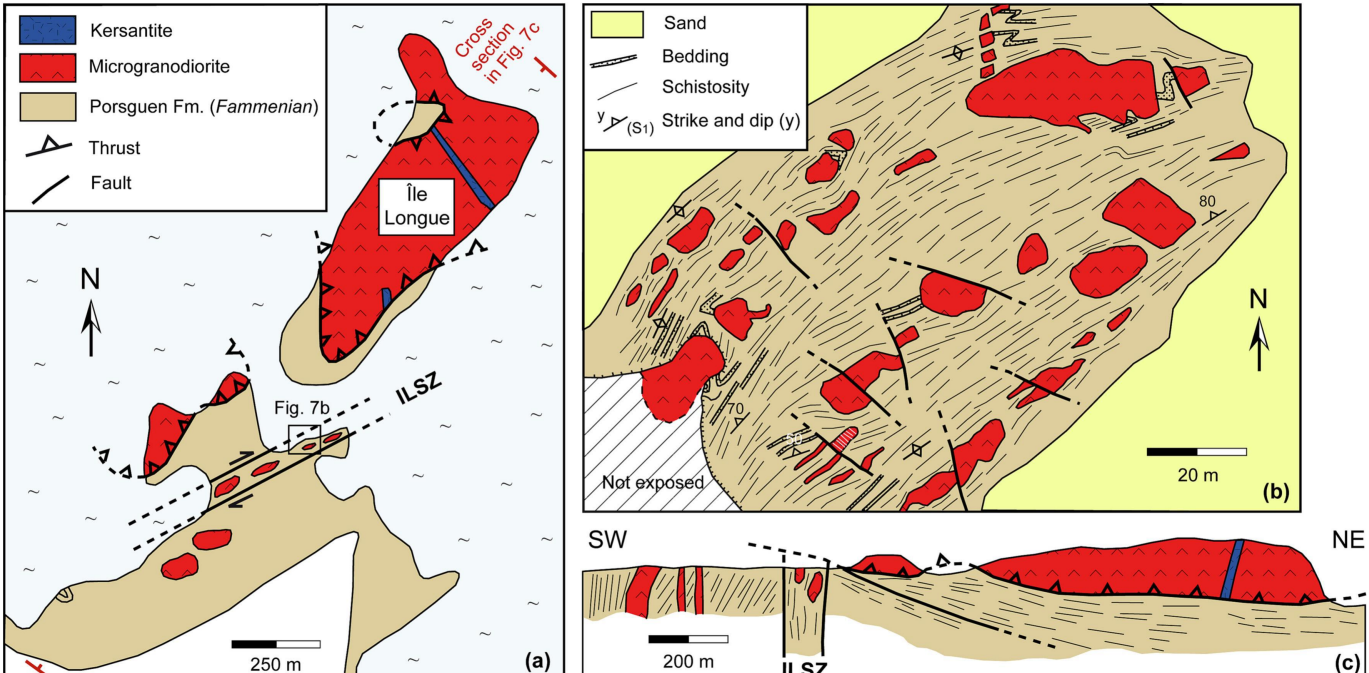
Kersantite
Microgranodiorite
Porsguen Fm. (Fammenian)
Thrust
Fault
Cross section in Fig. 7c
Île Longue
N
Fig. 7b
ILSZ
250 m
(a)
Sand
Bedding
Schistosity
Strike and dip (y)
y
(S1)
80
70
N
Not exposed
20 m
(b)
SW
NE
200 m
ILSZ
(c)

Figure 7

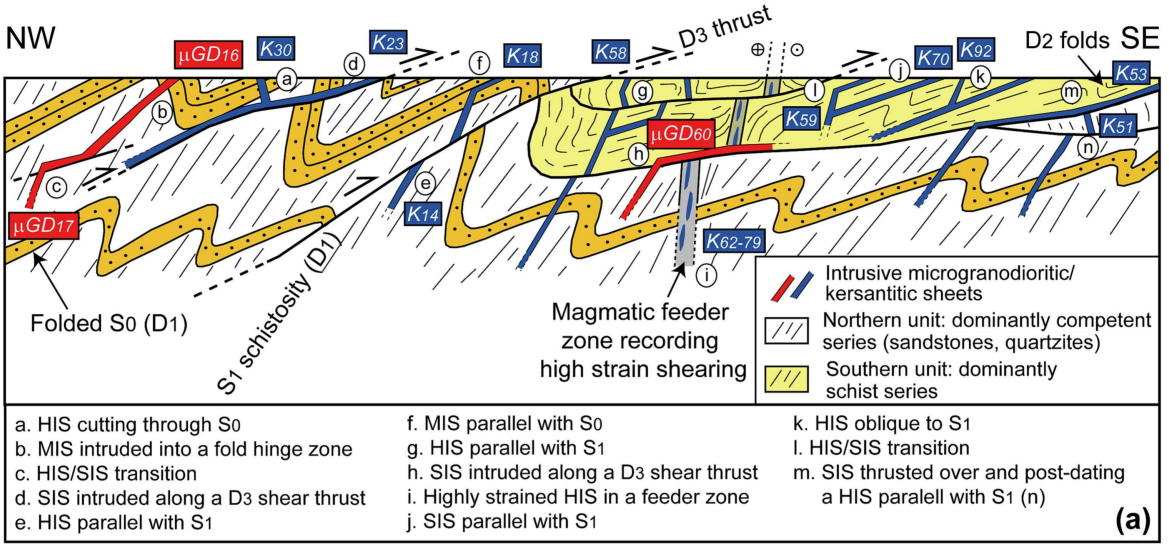
NW
SE
μGD16
K30
K23
K18
K58
D3 thrust
K70
K92
D2 folds
K53
K59
μGD60
K51
μGD17
K14
K62-79
Folded S0 (D1)
S1 schistosity (D1)
Magmatic feeder zone recording high strain shearing
Intrusive microgranodioritic/ kersantitic sheets
Northern unit: dominantly competent series (sandstones, quartzites)
Southern unit: dominantly schist series
a. HIS cutting through S0
b. MIS intruded into a fold hinge zone
c. HIS/SIS transition
d. SIS intruded along a D3 shear thrust
e. HIS parallel with S1
f. MIS parallel with S0
g. HIS parallel with S1
h. SIS intruded along a D3 shear thrust
i. Highly strained HIS in a feeder zone
j. SIS parallel with S1
k. HIS oblique to S1
l. HIS/SIS transition
m. SIS thrusted over and post-dating a HIS paralell with S1 (n)
(a)

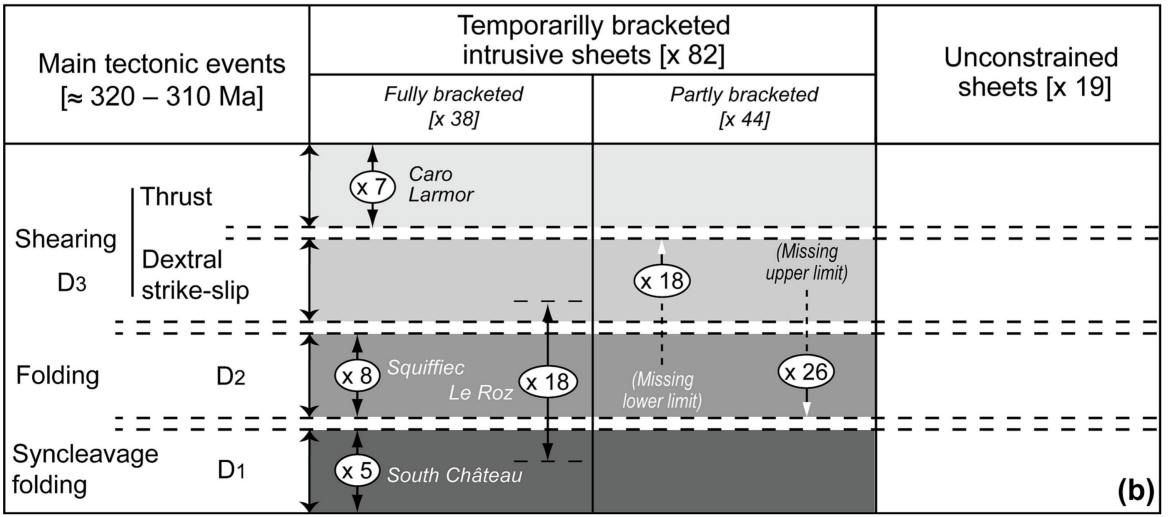
Main tectonic events [≈ 320 – 310 Ma]
Temporarilly bracketed intrusive sheets [x 82]
Fully bracketed [x 38]
Partly bracketed [x 44]
Unconstrained sheets [x 19]
Shearing D3
Thrust
Dextral strike-slip
Folding D2
Syncleavage folding D1
x 7
Caro Larmor
x 18
(Missing upper limit)
x 8
Squiffiec Le Roz
x 18
(Missing lower limit)
x 26
x 5
South Château
(b)

Figure 8

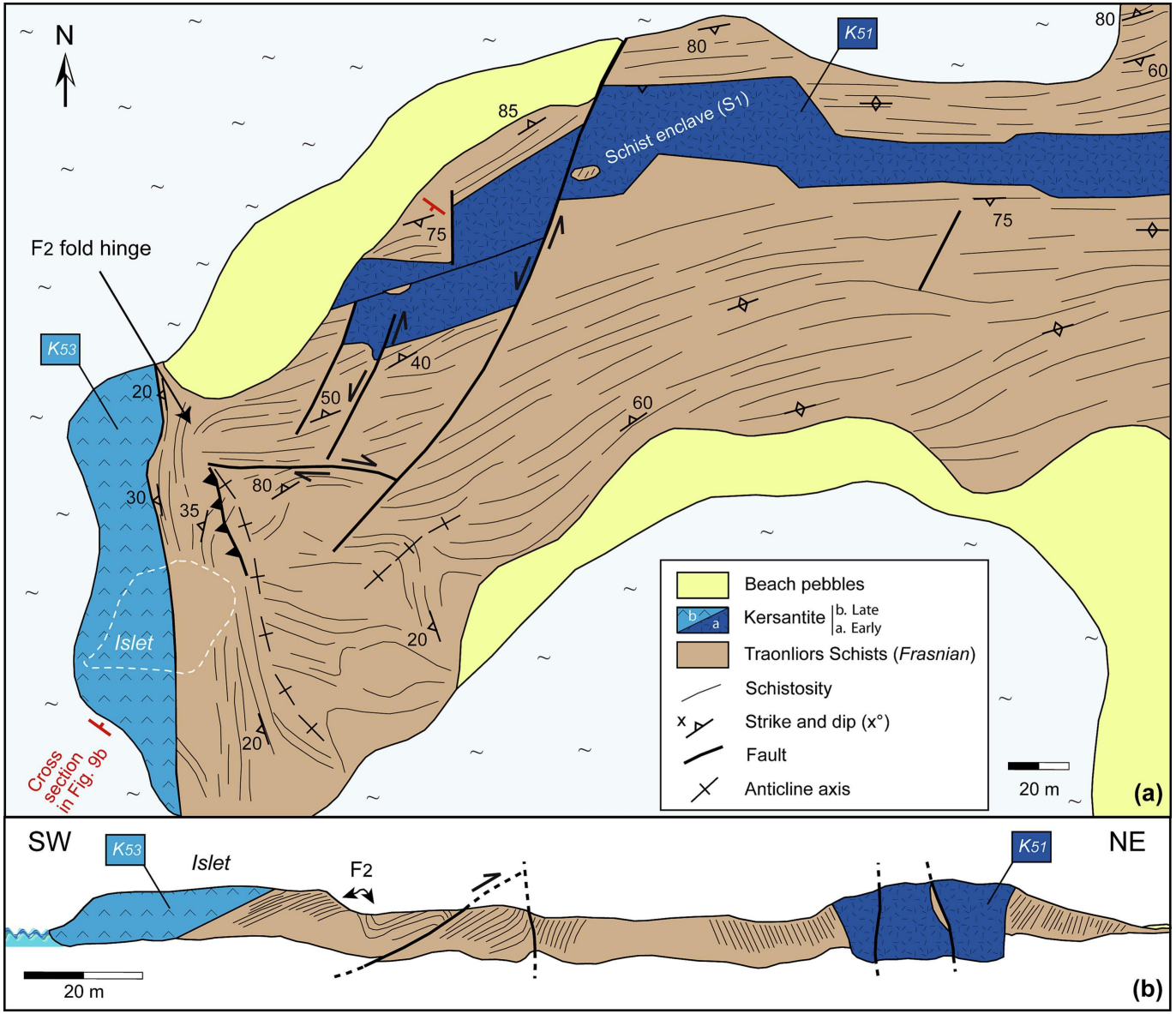
N
K51
K53
Schist enclave (S1)
F2 fold hinge
Islet
Cross section in Fig. 9b
80
85
75
40
50
60
20
30
35
Beach pebbles
Kersantite
b. Late
a. Early
Traonliors Schists (Frasnian)
Schistosity
Strike and dip (x°)
Fault
Anticline axis
20 m
(a)
SW
NE
F2
20 m
(b)

Figure 9

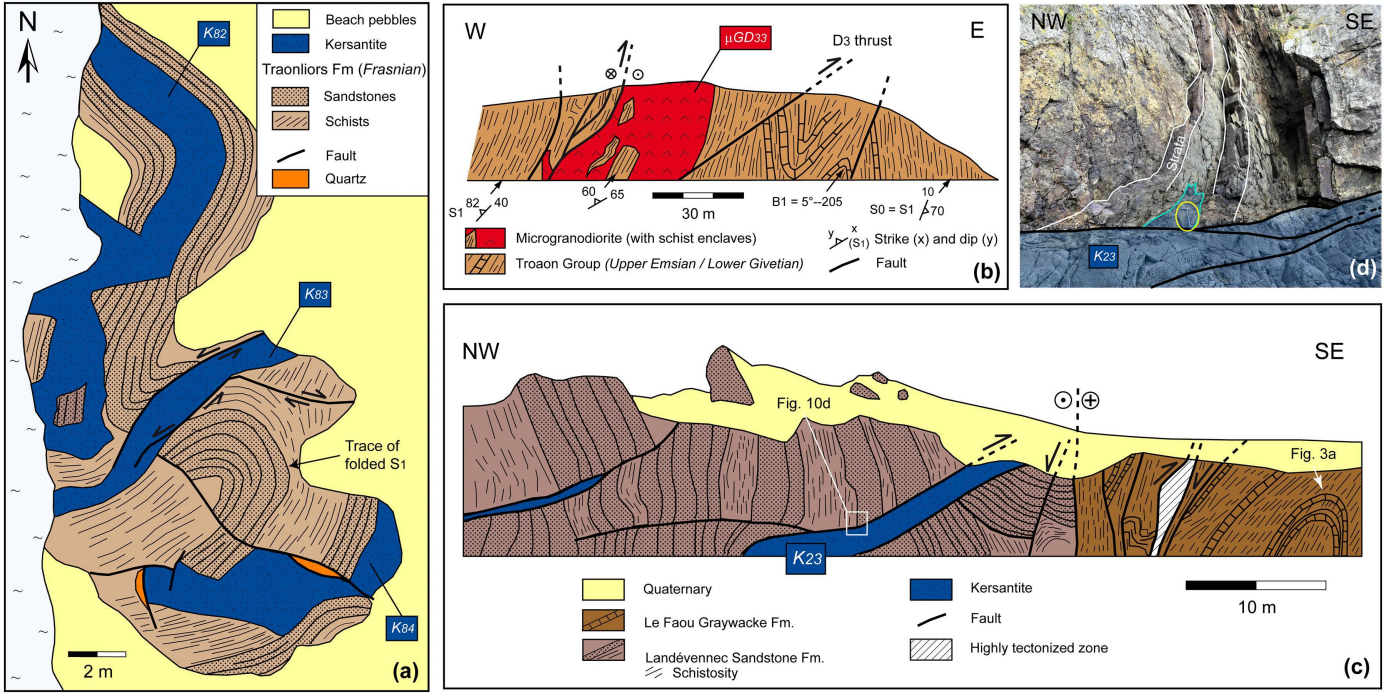
N
K82
K83
K84
Beach pebbles
Kersantite
Traonliors Fm (Frasnian)
Sandstones
Schists
Fault
Quartz
Trace of folded S1
2 m
(a)
W
E
µGD33
D3 thrust
S1 82 40
60 65
30 m
B1 = 5°–205
S0 = S1 10 70
Microgranodiorite (with schist enclaves)
Troaon Group (Upper Emsian / Lower Givetian)
(S1) Strike (x) and dip (y)
Fault
(b)
NW
SE
Strath
K23
(d)
NW
SE
Fig. 10d
Fig. 3a
K23
Quaternary
Le Faou Graywacke Fm.
Landévennec Sandstone Fm.
Schistosity
Kersantite
Fault
Highly tectonized zone
10 m
(c)

Figure 10

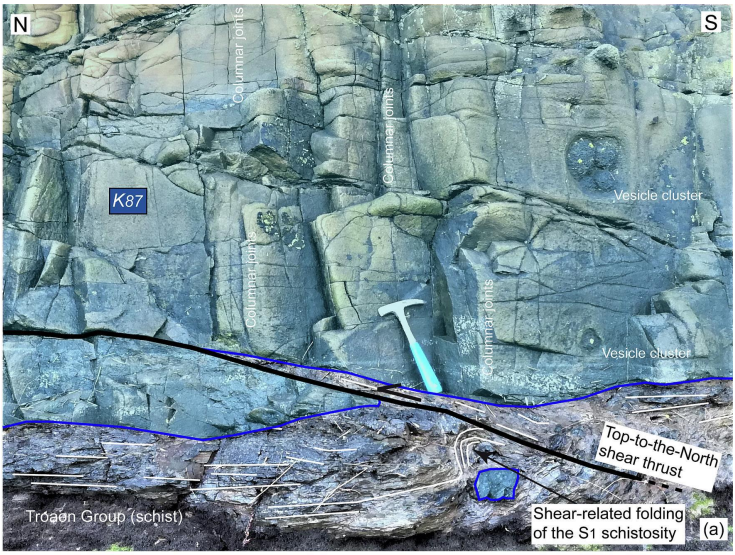
N
S
Columnar joints
Columnar joints
Columnar joints
Columnar joints
K87
Vesicle cluster
Vesicle cluster
Top-to-the-North shear thrust
Shear-related folding of the S1 schistosity
Troaon Group (schist)
(a)


N
S
K87
Schist enclave
(b)

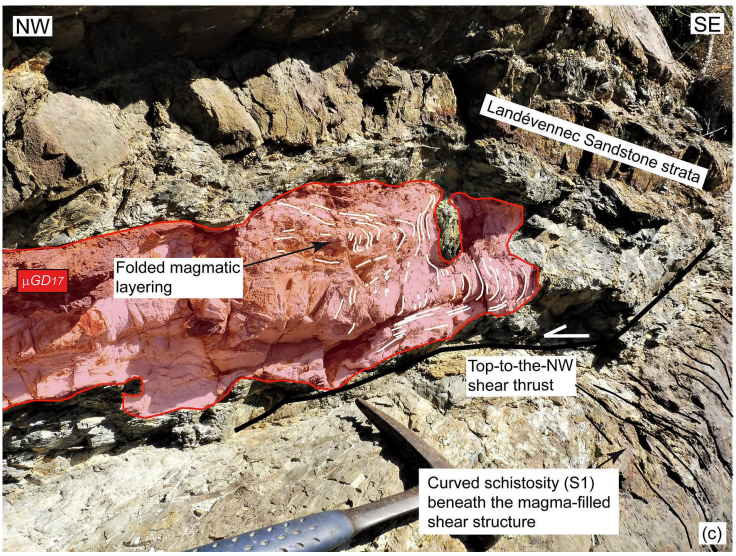
NW
SE
Landévennec Sandstone strata
μGD17
Folded magmatic layering
Top-to-the-NW shear thrust
Curved schistosity (S1) beneath the magma-filled shear structure
(c)

Figure 11

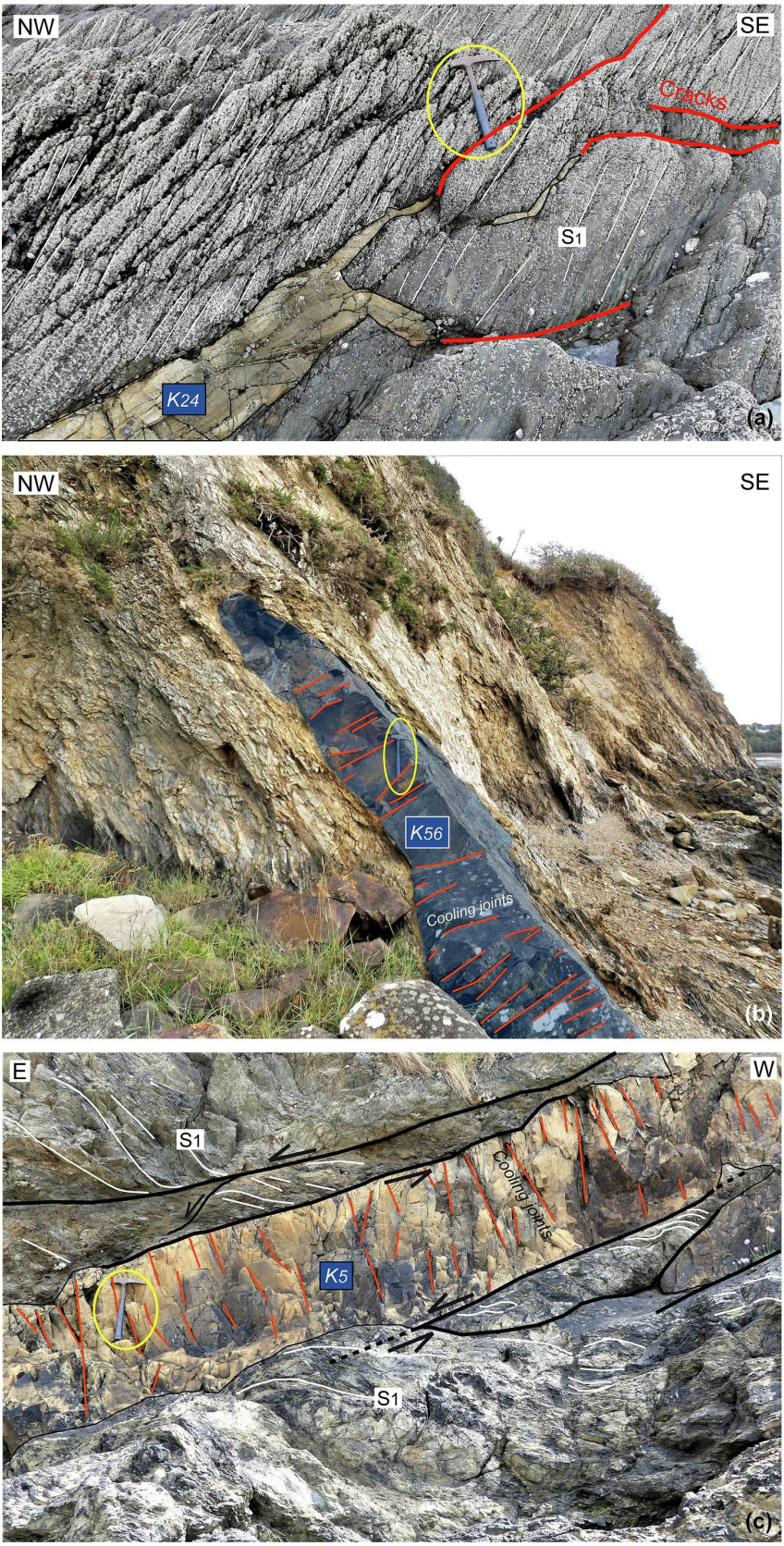
NW
SE
Cracks
S1
K24
(a)
NW
SE
K56
Cooling joints
(b)
E
W
S1
Cooling joints
K5
S1
(c)

Figure 12

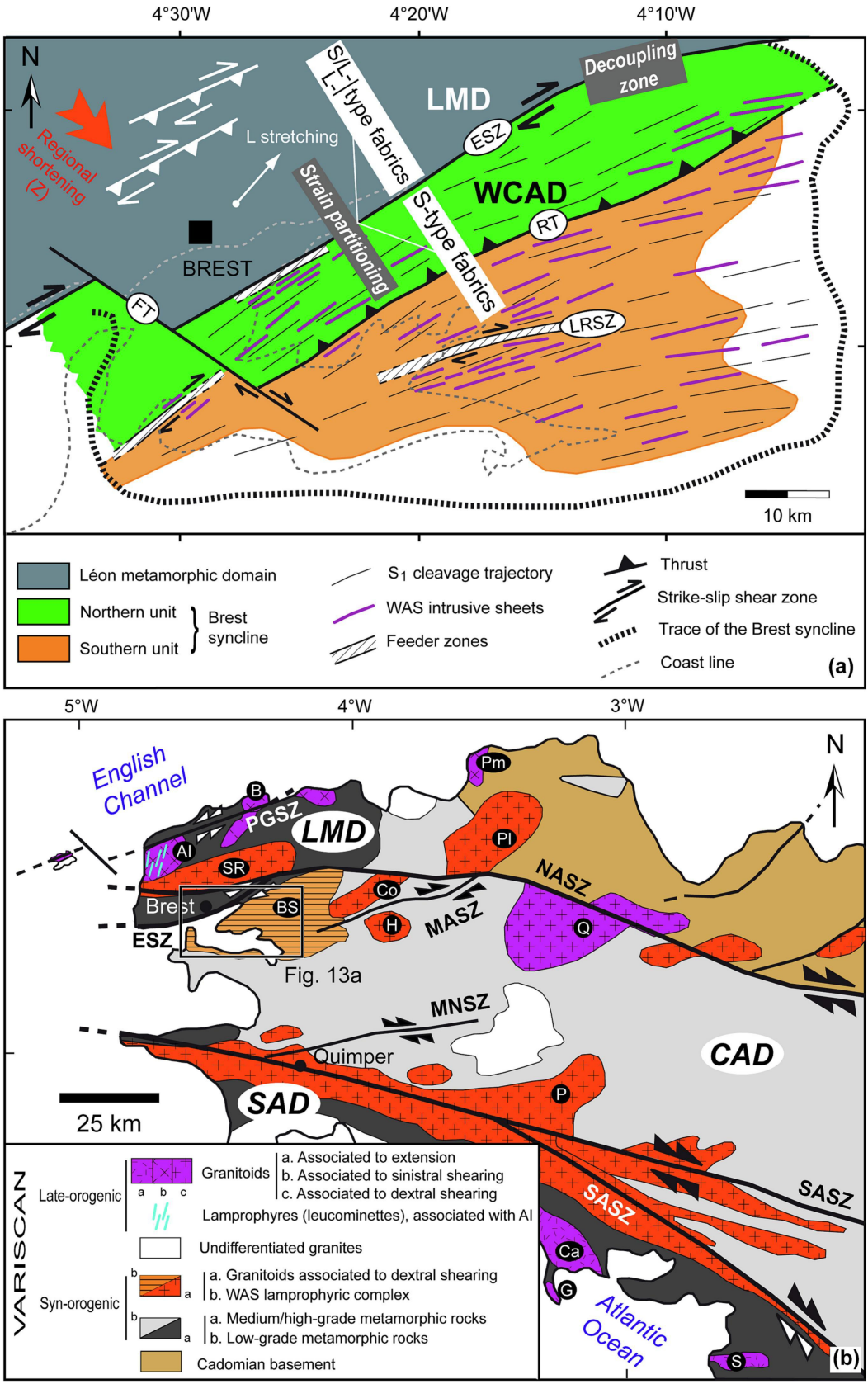
4°30'W
4°20'W
4°10'W
48°10'N
48°20'N
N
Regional shortening (Z)
L stretching
S/L-|type fabrics
L-|type fabrics
Strain partitioning
S-type fabrics
LMD
Decoupling zone
ESZ
WCAD
RT
BREST
FT
LRSZ
10 km
Léon metamorphic domain
Northern unit
Southern unit
Brest syncline
S1 cleavage trajectory
WAS intrusive sheets
Feeder zones
Thrust
Strike-slip shear zone
Trace of the Brest syncline
Coast line
(a)
5°W
4°W
3°W
48°N
English Channel
B
PGSZ
LMD
Pm
Pl
Al
SR
Brest
BS
ESZ
Co
H
MASZ
NASZ
Q
Fig. 13a
MNSZ
Quimper
CAD
SAD
P
25 km
SASZ
SASZ
Ca
G
S
Atlantic Ocean
(b)
VARISCAN
Late-orogenic
Granitoids
a. Associated to extension
b. Associated to sinistral shearing
c. Associated to dextral shearing
Lamprophyres (leucominettes), associated with Al
Undifferentiated granites
Syn-orogenic
a. Granitoids associated to dextral shearing
b. WAS lamprophyric complex
a. Medium/high-grade metamorphic rocks
b. Low-grade metamorphic rocks
Cadomian basement

Figure 13

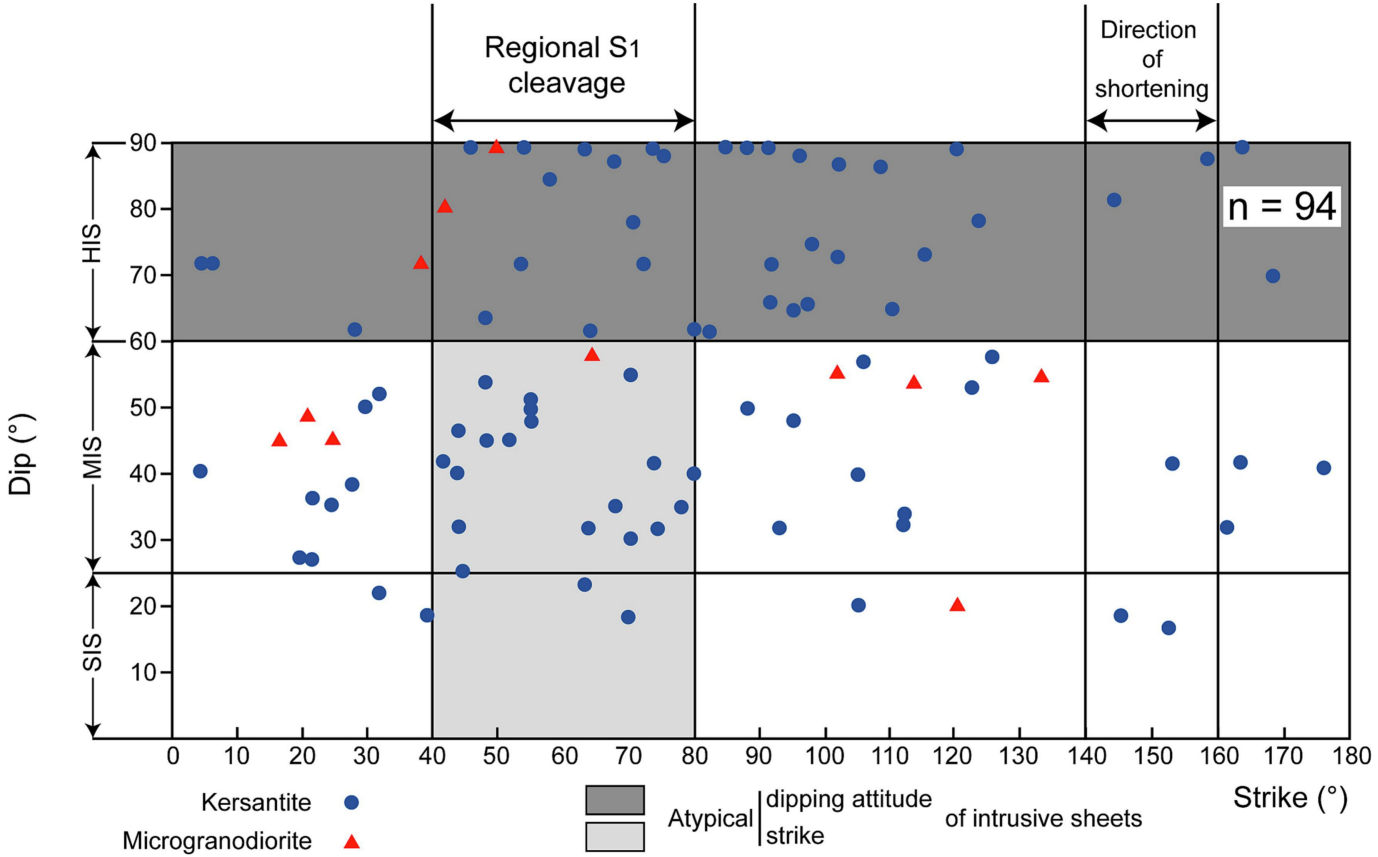
Regional S1 cleavage
Direction of shortening
n = 94
HIS
MIS
SIS
Dip (°)
Strike (°)
Kersantite
Microgranodiorite
Atypical dipping attitude strike of intrusive sheets

Figure 14

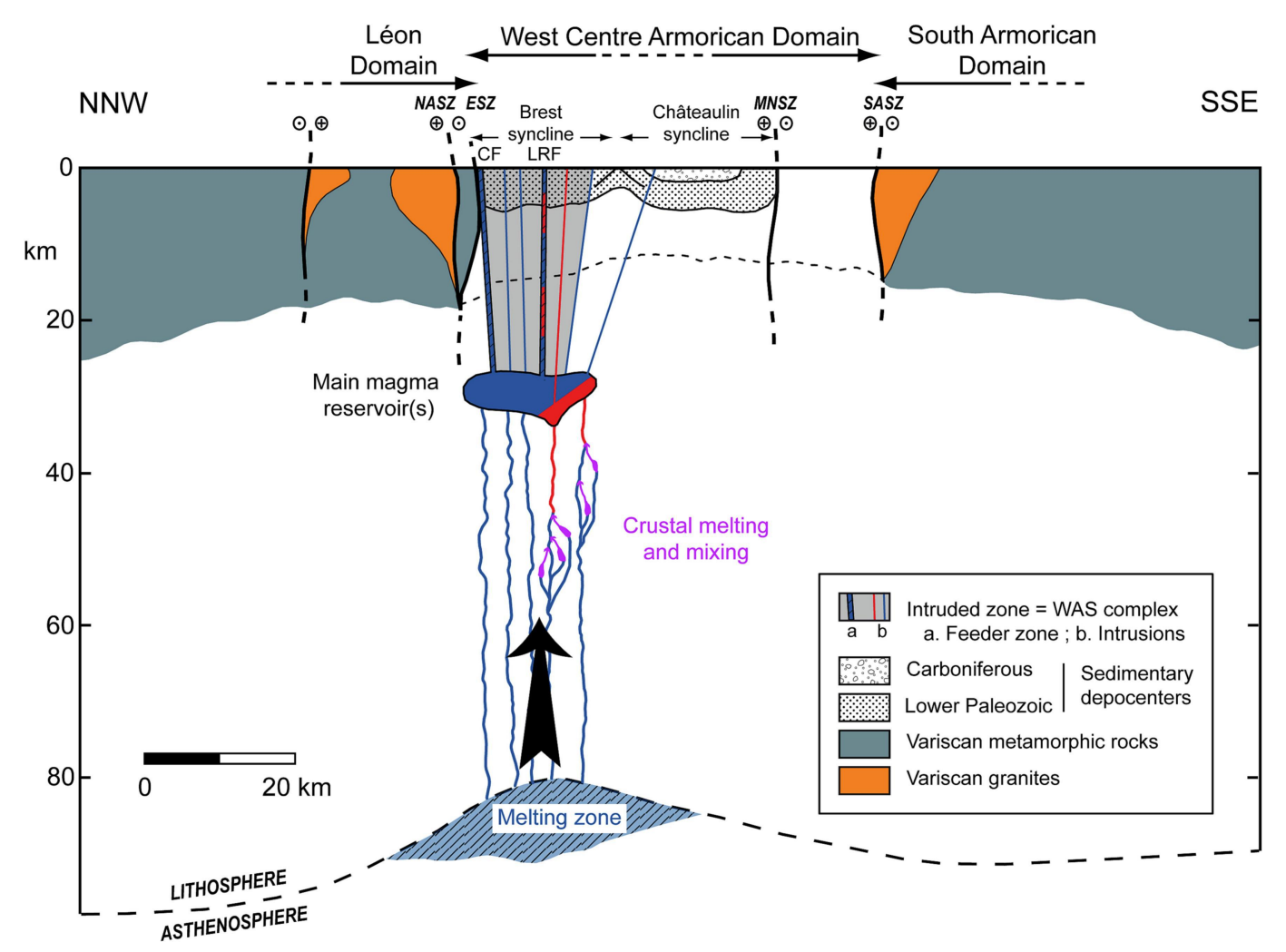
Léon Domain
West Centre Armorican Domain
South Armorican Domain
NNW
SSE
NASZ
ESZ
Brest syncline
CF
LRF
Châteaulin syncline
MNSZ
SASZ
0
km
20
40
60
80
Main magma reservoir(s)
Crustal melting and mixing
0
20 km
Melting zone
LITHOSPHERE
ASTHENOSPHERE
Intruded zone = WAS complex
a. Feeder zone ; b. Intrusions
a
b
Carboniferous
Lower Paleozoic
Sedimentary depocenters
Variscan metamorphic rocks
Variscan granites

Figure 15